Technical Report
AVES II

Team 01 Technical Report to the 2022 EuRoC

Aerospace Team Graz (ASTG)
Technical University Graz, Austria

Graz, October 3, 2022

Project Lead: Daniel Teubenbacher

Head of PCB: Sebastian Liebhart
Head of CAD: Kevin Posch
Head of Payload: Dorothea Krasser

Aerostructure: Felix Kerschbaumer (Module Lead), Felix Steinwender (Module Lead), Georg Witzlinger (System Engineer), Steven Nittel (System Engineer), Johannes Binninger, Jana Gillmayr, Nemanja Ristic

Avionics: Thomas Köhler (Module Lead), Tim Sagaster (Flight Computer Lead), Christian Jäger (Telemetry Lead), Stefan Weiß (System Engineer), Kirsten Stefanie Ziegler (Software System Engineer), Johannes Becker, Raffael Bischof, Harald Deutschmann, Jakob Faltisek, Kristian Fleck, Jakob Fuchsberger, Jakob Herk, Max Jost, Andre Koczka, Clara Lindner, Stefan Reisinger, Lorenz Ruprecht, Patrick Schuster, Oleksii Shekhovtsov, Michael Siemmeister, Gregor Steinbauer, Andreas Steiner, Zan Ulaga, Thomas Weber, Christiane Woletz, Michael Zweimüller

Propulsion: Daniel Kaiser (Module Lead), Sunny Laddha (System Engineer), Markus Baumgartner-Steinleitner, Tobias Dorn, Michael Hofer, Valentin Nimmervoll, Michael Ortner, Cindy Resch, Christoph Swoboda, Philomena Vatter, Felix Wögerbauer

Recovery: Manuel Obernberger (Module Lead), Manuel Nestler (System Engineer), Matthias Andergassen, Máté Györffy, Viktoria Keusch, Alexandra Linhart, Lukas Reinisch, Thomas Riegelnegg, Jakob Rupitz

Marketing: Ricarda Auer (Module Lead), Lena Grupp, Vivian Posch

System Administrator: Maximilian Anrather

Safety Officer: Markus Baumgartner-Steinleitner

Aerospace Team Graz - Board 2022

President:	Stefan Weiß
Vice President:	Georg Witzlinger
Treasurer:	Dorothea Krasser
Vice Treasurer:	Thomas Köhler
Secretary:	Manuel Obernberger
Vice Secretary:	Matthias Andergassen

Abstract

After our inaugural participation in the European Rocketry Challenge in 2021, the Aerospace Team Graz returns this year with a larger rocket, built by a bigger team. Designed for the 3 km solid SRAD (S3) category, AVES II maintains the "Student Researched and Developed" philosophy at its core and builds on the knowledge and success of its predecessor AVES. In addition to the mandatory flightcomputer (Eggtimer), this years payload features three CubeSats, of which two are built entirely by polytechnic high school teams. Thus, we continue sharing our enthusiasm for rocketry with the next generation and maintain the successful cooperation initiated last year. Moving further down along the rocket, the payload in the nosecone is followed by the Recovery Module, which consists of a two-stage deployment system and relies on a main and drogue parachute. Located beneath is the avionics section – the brain of the rocket. It comprises the power supply, telemetry system (antennas), camera system, black box, and most importantly, the self-designed and built flightcomputer, which works with an improved version of the self-developed real time operating system RavenOS. Separated from the Avionics Module by an empty volume, the airbrake provides more precise control after the engine burnout for reaching our target altitude of 3 km. While the Propulsion Module at the bottom of the rocket continues to be powered by Rocket Candy (mixture of potassium nitrate and sorbitol), it has been greatly improved compared to its predecessor and is thus one of the highlights of AVES II. A new production process and design geometry allow the direct casting of a single fuel grain to create a booster with high reliability and repeatability. Furthermore, a special sensor bay at the top end of the booster enables the monitoring of the combustion process. All of these modules are integrated into a housing composed of carbon fiber and also glass fiber to ensure radio frequency transparency for communication with the self-developed groundstation. The development phase was greatly supported by data gained through extensive testing of the rocket with a custom-built test-stand and detailed numerical simulations. Thus, we are confident that AVES II will achieve its mission of completing an instrumented flight to an altitude of 3 km and safely landing back on the ground. Furthermore, we have set ourselves the goals to produce an excellent technical documentation and win at least one of the awards at EuRoC. In any case, we are proud to have grown as a team in terms of members, as well as knowledge and experience.

Godspeed to all teams!

Contents

1. Introduction

The Aerospace Team Graz (ASTG) was founded in late 2019 as a non-profit organization by a few motivated mechanical engineering students of the University of Technology Graz (TUG) in Austria. Their vision was to build a completely self-designed rocket and participate in international rocketry competitions. In the beginning, the team started with a prototype rocket that was meant to reach an apogee of 1 km and gained important experience on general rocket design and development. The ASTG grew rapidly to 65 members in 2021 and initiated the project AVES, a solid propellant rocket that was designed to reach an apogee of 3 km at the European Rocketry Challenge (EuRoC) 2021. The rocket launch of AVES in Portugal last year was the team's first launch and was actually very successful too: the main goals of the project were to successfully launch the rocket and to win the award for the best technical documentation at EuRoC 2021. Despite having achieved these main goals, there was of course room for overall improvement, e.g. in landing rockets - safely.
Today, while the vision has not changed, our team has grown to around 80 students from almost all academic institutions in Graz (University of Technology Graz, University of Graz, FH Joanneum Graz, Campus 02, Montantuniversitaet Leoben). While most of the students are enrolled in technical studies at the TUG, we are proud to represent many different fields as can be seen in the following Figure 1.

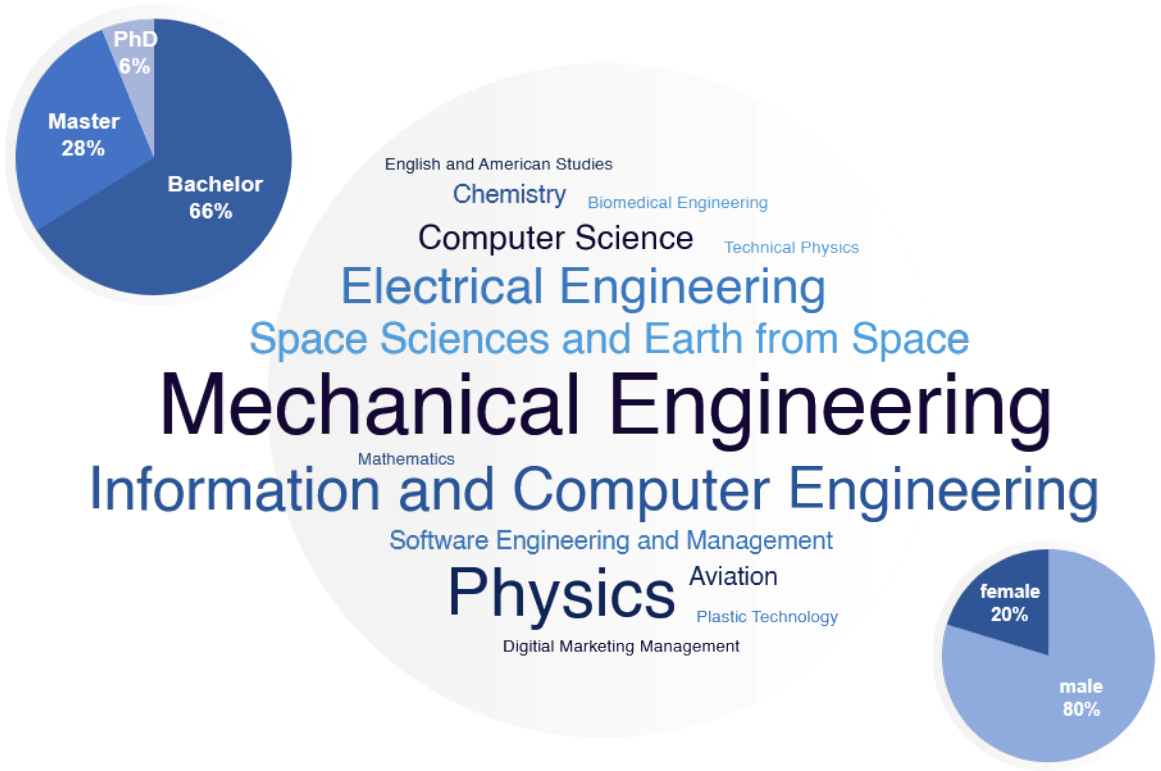

Figure 1: Schematic diagram of all the fields of study represented by the ASTG as well as study progression and gender distributions

In Figure 1, one can also see the progression of the students, where most are at a bachelor level. The team is not only diverse in terms of different fields of study, but it also aims to motivate anyone who is interested, regardless of origin or gender. In fact, the percentage of women in the team increased to 20 % this year and is still growing. Moreover, more than ten nationalities are represented in the team.

The ASTG is structured mainly into two teams, the *Rocket Team* and the *Business Team*. These split up further into smaller working groups called modules, as illustrated in Figure 2.

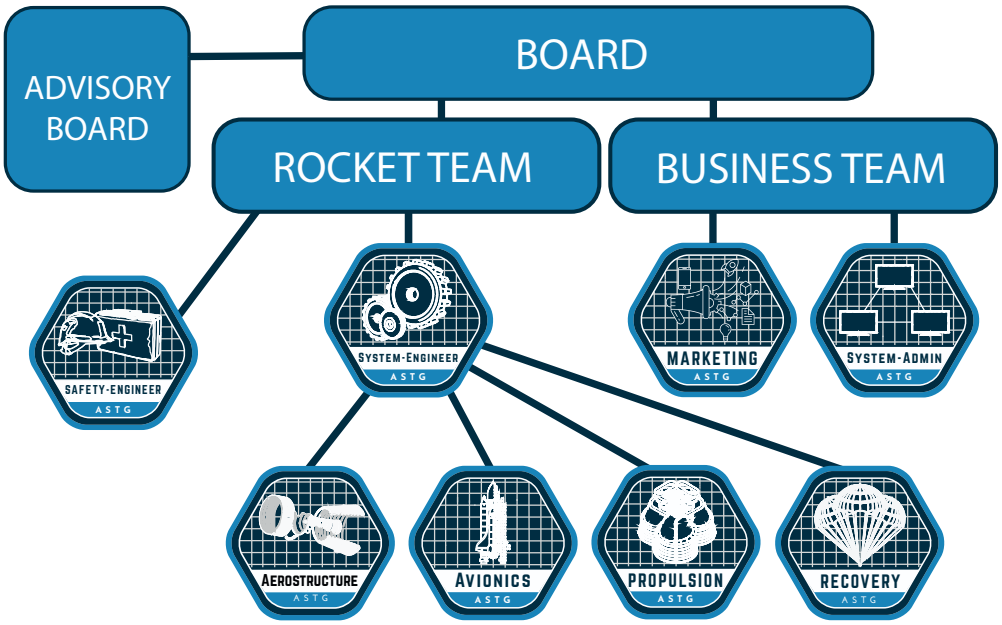

Figure 2: Team structure of the ASTG

The *Business Team* is divided into Marketing and System Administration. The Marketing Module ensures that the ASTG is well represented on various social media platforms and is responsible for the newsletter that is sent out regularly to our sponsors. They also deal with the organization of conferences and focus on team building and launch events. The System Administration Module deals with all IT related issues such as program licenses and (cloud) data storage.
The *Rocket Team's* modules are defined by the different subsystems of the launch vehicle. The Aerostructure Module (AST) is responsible for the basic flight stability of the rocket and the aerodynamic design from the nosecone to the fins at the tail. Possible Control Actuator Systems (CAS), e.g. for aerodynamic braking, are also developed by this module. Moreover, Aerostructure deals with the integration of all other subsystems into the outer skin and basic structure of the rocket, the balancing of the center of gravity and also weight optimization. In Avionics (AVI), everything revolves around the electronic hardware and software of the rocket, working on sensors and the main computer, as well as dealing with the control of the rocket, data transmission and visualization. The rocket engine is designed and manufactured by the Propulsion Module (PRO), which entails dealing with additive manufacturing processes, different materials and simulations, among many other things. Parachutes, and their anchoring and ejection systems are developed in the Recovery Module (REC) so that the rocket can safely return to the ground. In addition to the technical working groups, the System Engineers coordinate and optimize the overall process ranging from project-, risk- and time-, to resource management. Finally, our Safety Officers ensure the safety of the entire team while testing and handling hazardous substances.

All the development processes, manufacturing and testing of our rocket components would not be possible without our partners and suppliers. Our main sponsors include the University of Technology Graz, European Space Agency Space Solutions Austria (ESA Space Solutions Austria), the Institute of manufacturing engineering (IFT), the Institute of Innovation and Industrial Management (IIM), Astotec Pyrotechnic Solutions, PEAK Technology, Zirkonzahn and many more. We are very grateful for the collaborations with more than 50 companies and institutes and their support even in challenging times with chip shortages and material delivery bottlenecks.

2. Project Goals and Mission Objectives

Despite not being a required chapter for this technical report, it is still important to quickly summarize the main AVES II project goals and principal mission objectives in order to fully understand the system architecture, design decisions and testing procedures.

2.1. Main Project Goals

- Maintain the good documentation that won us the technical award at EuRoC 2021 to help current and future ASTG team members.
- Successfully accomplish the launch, flight and safe recovery of AVES II at a flight test and at EuRoC. (two flight models are built)
- Gather data and camera footage during flight.
- Win an award at EuRoC 2022!

2.2. Principal Mission Objectives

- Create and build a sustainable 3000 m launch platform for a 3x1U CubeSat payload of 4 kg. The payload shall consist of multiple projects from secondary technical schools and from the ASTG.
- Advance SRAD solid propulsion for sounding rockets, in terms of building the most predictable and reliable Rocket Candy booster.
- Inspire and motivate people not only from the ASTG, but also from the broader community for rocketry, science and engineering in general.

3. System Architecture

3.1. Overview

The system concept of AVES II comprises four main modules, which work together seamlessly to fulfill the mission objectives. Firstly, the solid propellant rocket motor of the Propulsion Module is designed to aim higher than the target height of 3000 m. This allows the Avionics Module to regulate the rocket's flight apogee with the help of the airbrake, which is part of the Aerostructure Module. After passing the apogee, the avionics system signals the recovery system to sequentially deploy the drogue and main parachute, to ensure a safe landing of the rocket. The main modules themselves consist of several components that are described in detail in the subsequent sections. The rocket is complemented by a groundstation, which receives all sensor data during the flight.

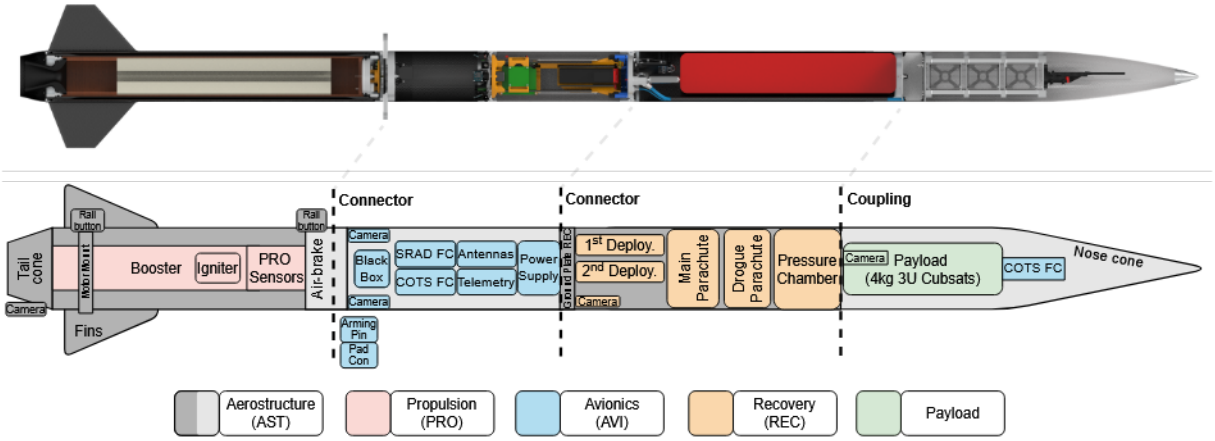

Figure 3: Rendering of AVES II (top) and schematic diagram (bottom) of the general arrangement of main system components.

A schematic overview of the general arrangement of the rocket components is illustrated in Figure 3. Starting from the left, the bottom part of the rocket houses the instrumented solid rocket motor. Moving to the right, the next part is the airbrake. The middle section of the rocket features the brain of the rocket, namely the Avionics Module, which includes the flightcomputers, black box, arming pin, pad connection, antennas, cameras, telemetry and power supply system. The payload, comprising three 1U CubeSats, and a redundant flightcomputer are placed inside the nosecone in the top section of the rocket (far right). The latter can be separated to allow the Recovery Module, which rests directly beneath the payload, to deploy the parachutes. All these parts are integrated into a five-part shell. The rocket dimensions, total mass, as well as the main performance figures (from OpenRocket) are listed in Figure 1, detailed system data is shown in Appendix B.

Table 1: AVES II dimensions, mass and performance figures.

Characteristic	Value
overall length	3528 mm
diameter	152.4 mm
span width	435 mm
mass (wet)	33.8 kg
propellant mass	9.5 kg
total impulse	11 000 Ns
acceleration (max)	15 g
velocity (max)	316 m/s
velocity (off-rod)	44 m/s
apogee w/o airbrake	3500 m
ground hit velocity	6 m/s

AVES II uses a SRAD flightcomputer and a COTS flightcomputer to determine flight phases, actuate the airbrake and to redundantly trigger the recovery events as will be explained in detail in Chapter 3.5. The ignition system that can be used with a wire and wireless as well as the telemetry system is described in Chapters 3.7 and 3.6. Following Figure 4 gives an overview of the electrical and software components and communication inside and outside the rocket.

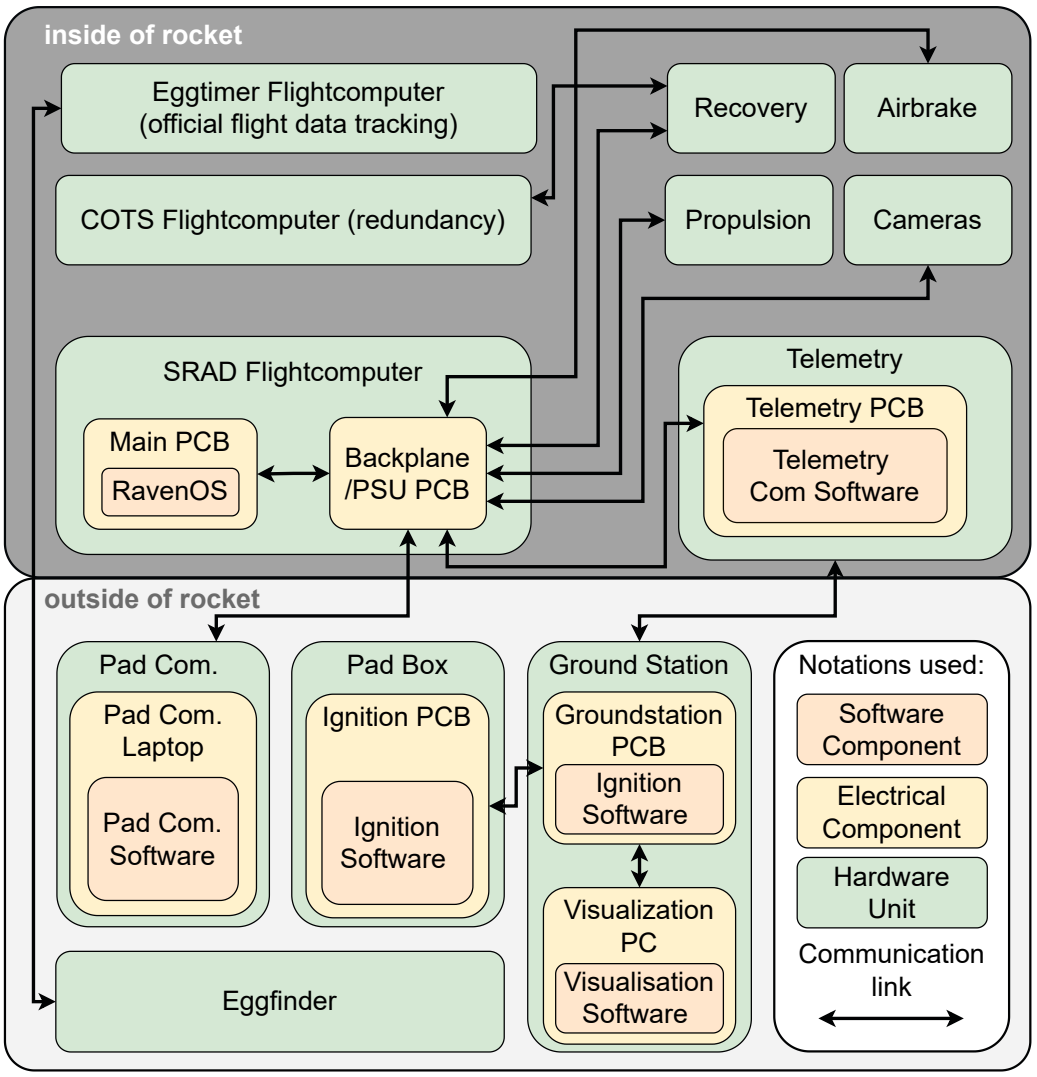

Figure 4: AVES II electrical and software system diagram.

3.2. Propulsion Subsystem

The propulsion system of AVES II, like its predecessor AVES, contains a solid fuel motor, based on a potassium nitrate/sorbitol propellant. To achieve the propulsion system's goal of developing an instrumented, reliable and reusable booster for the rocket, the design was completely redeveloped. Based on preliminary simulations, a new geometry for the fuel grain was chosen, which was also the main design driver for the booster structure. An overview of the boosters main characteristics can be found in Table 2 below. In addition, an overall view of the booster can be seen in Figure 5.

Table 2: main booster characteristics

Characteristic	Value
outer diameter (max)	135 mm
inner diameter	120 mm
casing length	1000 mm
maximum expected combustion pressure	35 bar
nominal operating combustion pressure	20 bar
nominal operating combustion temperature	1200 °C
total impulse	11 000 Ns
burn time	3.5 s
throat diameter	38 mm
fuel mass	9500 g
empty mass	6700 g

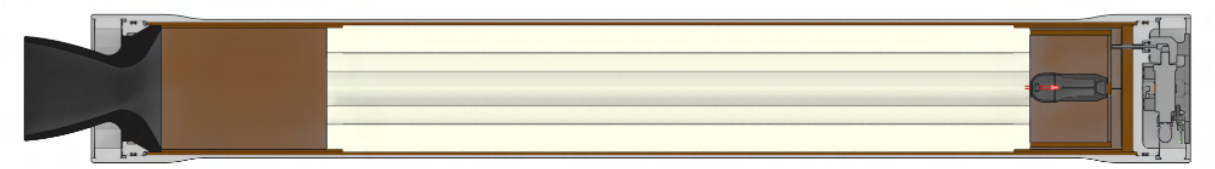

Figure 5: cross section of the solid rocket booster of AVES II

3.2.1. Booster Design

Structure

The main structure of the booster is formed by an aluminum tube of the alloy EN AW 6082. To reduce the weight of the shell, it was machined on the outside to reduce the wall thickness, making it two-thirds lighter than the stock material. A Finite Element Analysis (FEA) was conducted to optimize the weight reduction while ensuring its structural integrity (see Appendix G.1). On each end a tight fit for the O-Ring and an internal thread seal the combustion chamber and absorb the axial forces generated by the pressure. In these internal threads, a retainer ring is screwed in, holding the internal structure together. The reusable graphite nozzle is held by the aluminum nozzle holder via a conical interface, which not only transmits the forces but also seals the combustion chamber with the help of graphite paste. A CFD analysis of the combustion gases inside the nozzle delivered pressure data, which were then used as a load in a FEA for the nozzle, as can be seen in the Appendix E.2. For graphite nozzles it is essential to avoid any notches that can cause stress peaks in the material and lead to a brittle fracture, as experienced during the development of AVES. In Figure 6 a cross section of the nozzle assembly can be seen. When assembled, the nozzle presses against the post combustion chamber insulation, which is glued into the main insulation and is also overlapped by the fuel grain, ensuring no leakage of any combustion gases. As mentioned above, a Fluorinated Rubber (FPM) 80 shore o-ring between the nozzle holder and the main booster tube seals the system.

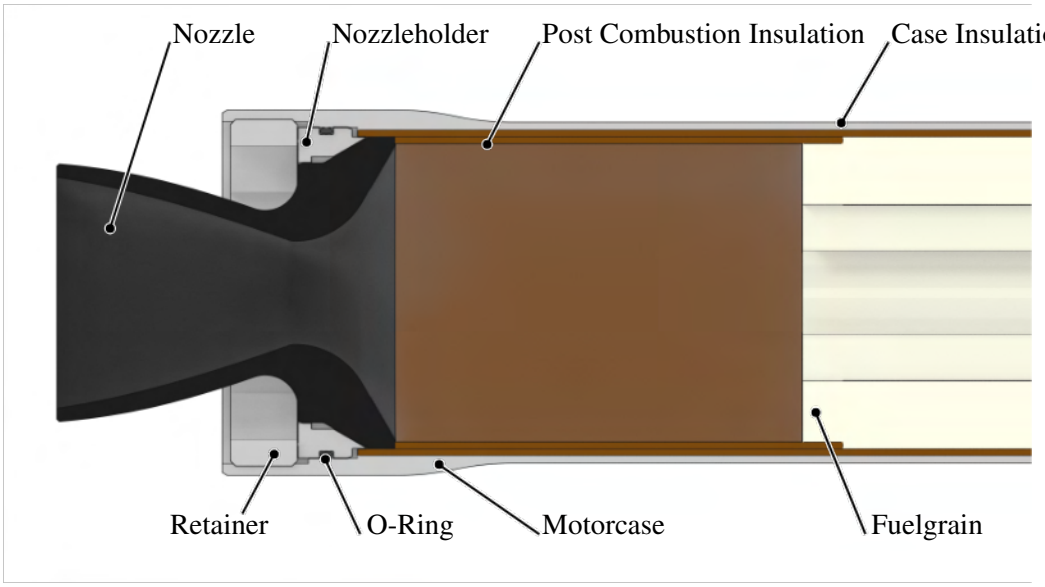

Figure 6: Detailed view of the nozzle section.

On the opposite side of the nozzle a bulkhead made of aluminum ensures the closure of the system. In addition, it features openings for a pressure sensor and thermocouple, a mount for the 3D-printed instrumentation unit and a cable for the grounding. The weight of the bulkhead was also optimized based on a FEA (see Appendix E.2). The insulation for the bulkhead is made of carbon layered cork, whereby an ablative layer of carbon prevents the cork from burning, while the cork itself provides the thermal insulation. The bulkhead section (see Figure 7) in particular must not exceed a certain temperature as it would damage the electronics, sensors and 3D-print.

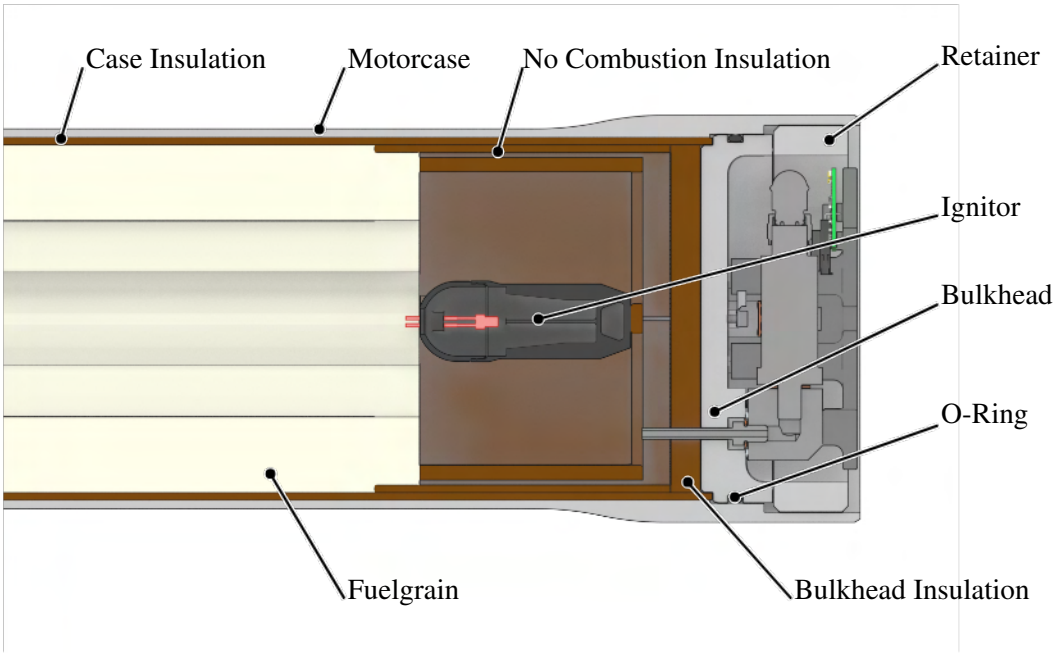

Figure 7: Detailed view of the bulkhead section.

The main insulation of the booster is comprised of a phenolic-cotton-composite tube, which at the same time is the carrier material for the fuel grain. As the post combustion chamber of the booster is exposed to the combustion gases, an additional insulation tube, named "No Combustion Insulation", is glued into the main insulation, securing the fuel grain and protecting the aluminum tube.

Data Processing Unit

As the instrumented booster uses analog sensors for all measurements, it was necessary to convert them into digital signals locally, as not to create additional noise over the length of the wires, while rendering it a more independent subsystem for future usage. Based on the experience with our booster testbed, the same input amplifiers and analog-digital-converter were implemented on a compact PCB located in the bulkhead section. The connection to the rest of the rocket is made when inserting the booster, utilizing a custom made plug and socket connection, with its counterpart mounted to the bottom of the airbrake. All parts are mounted using an ABS 3D-printed structure, which also provides rotational alignment. The two sensors used to measure the internal state of the combustion are a thermocouple type K and a Adroit 6200 pressure transducer. The thermocouple is screwed directly into the bulkhead by a M8x1 thread, and sealed with a copper washer on the top as well as high temperature silicon on the bulkhead insulation.

Measuring the pressure of a solid rocket motor entails two main challenges, the high temperature and the dirty combustion gases, which contain a lot of unburned material or residues from the combustion. For weight optimization, a pressure capillary tube was used to protect the pressure sensor from the high temperature gases. As pressure builds up inside the combustion chamber, the hot gases compress the air inside the capillary tube, until the pressure remains constant.. At this state, as no fluid flow is present, no more hot combustion gases can enter the capillary tube. This boundary layer, formed in the tube, protects the pressure sensor. A measurement of the temperature inside the pressure sensor is described in the 2nd hot-fire report (see Appendix C.3), proving the working principle of this system. A downside of this system is the clogging of the capillary tube, leading to a wrong pressure reading, whereby the pressure drop is much slower than in reality. To counteract this, several versions of the pressure capillary tube, in our case called “pressure needle”, were tested to avoid clogging as much as possible.

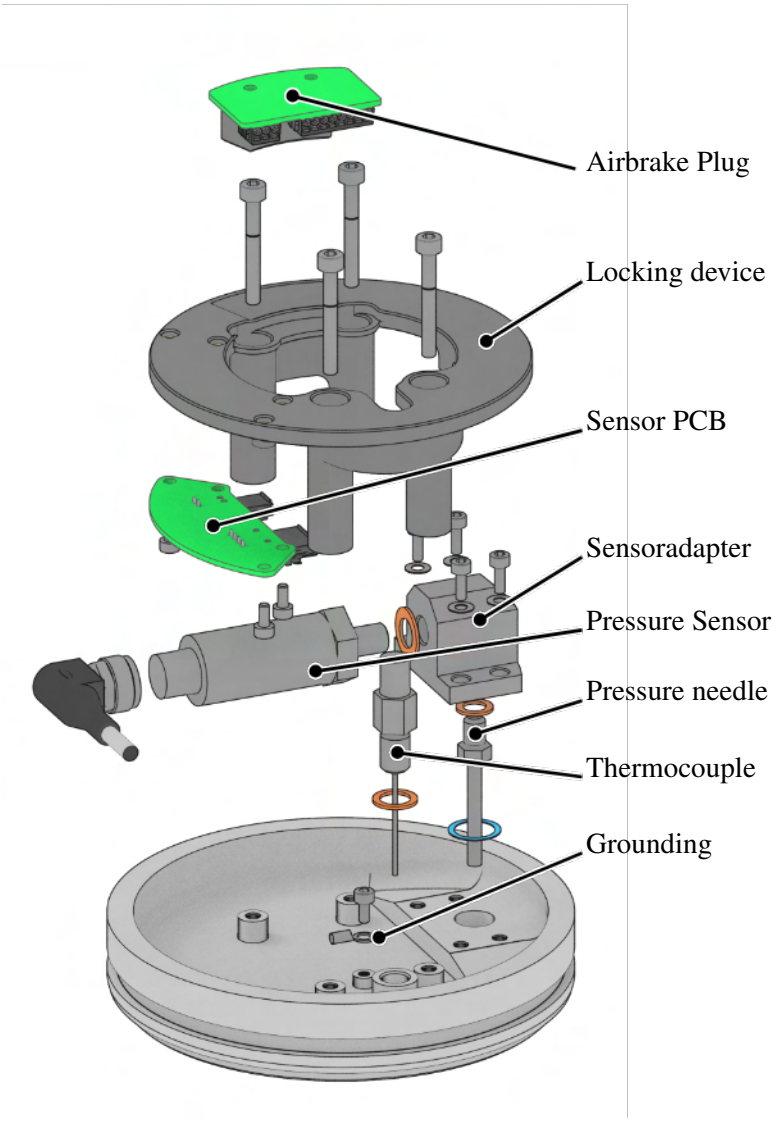

Figure 8: exploded view of the sensorbay

3.2.2. Fuel Grain

The main reasons for using Rocket Candy (RC), similar to last year, were the safety, accessibility in Austria and the already gained experience from the previous year. However, the “finocyl” geometry (6-point star as can be seen in Figure 12) was chosen as a new design for the grain geometry, mainly for

reasons of repeatability and time efficiency. This design has the significant advantage over the “bates” geometry of being castable in one piece and thus avoiding possible shifting of individual fuel grains during flight, incorrect assembly or hot spots between the grains. Besides the two main components of the propellant, a non toxic additive called Sodium Laureth Sulfate (SLS) was added to decrease the viscosity of the mixture, thus facilitating the casting.

Table 3: fuel composition

Component name	Weight parts [a.u.]
Potassium Nitrate (KNO_3)	65
Sorbitol	35
Sodium Laureth Sulfate (SLS)	0.3

Manufacturing Process

To increase the quality of the AVES II fuel grains, while saving resources and reducing complexity as compared to last year, the manufacturing process was completely redesigned (including methods and hardware) by one of our team members in the framework of his bachelor thesis. The result and thus the work flow of the redesigned manufacturing process can be seen in Figure 9.

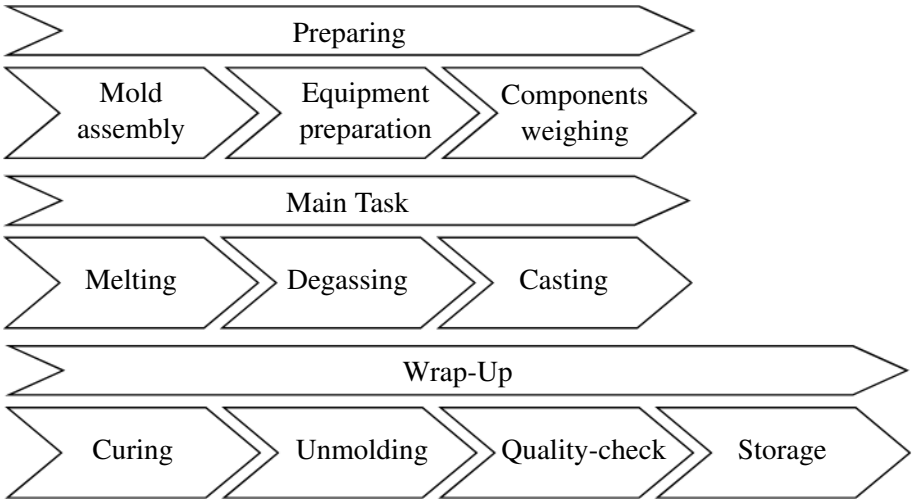

Figure 9: Work flow of the manufacturing process.

The production of the finocyl fuel grain is achieved by casting melted propellant directly into the insulation around a fixed mold with the corresponding geometry for the port. To facilitate the extraction of this mold after curing, it is composed of multiple detachable parts (3D-printed fins attached to an hexagonal aluminum core) as can be seen in Figure 10. The mold is assembled in the preparation phase and further laminated with PTFE and Kapton tapes to avoid adhesion of the RC. Weighing of the components includes the empty insulation tube to enable a determination of the propellant mass after curing.

As air enclosures in the cured fuel grains significantly degrade the repeatability of the booster performance (see more details further below), degassing was added to the main task between melting and casting. This however, required the conception of an container that is able to maintain vacuum and high temperatures uniformly. The solution, as displayed in Figure 11, was a double-walled pot (filled with glycerin for heat storage) with a special sealing lid attached to a vacuum pump. The pot was heated via a thermostat controlled induction plate for optimal temperature, and time efficiency. Additional time was saved by using an electric drill with a stirring attachment to mix the ingredients, thereby avoiding the preparation of finely ground ingredients (especially KNO_3 forms large clumps during storage). The excessive air that was introduced into the melted mixture by the stirring, posed no problem owing to the subsequent degassing.
To avoid voids and blowholes, the casting was done in multiple batches with a maximum of 2 kg of RC each, whereby a specially designed funnel was used to ensure a laminar flow of the molten propellant into the mold. Thus, the steps of the main task as illustrated in Figure 9 are repeated until the fuel grain acquires the required mass.
Due to the highly hydrophilic nature of RC, the fuel grain needs to be stored airtight during the 24 h of curing, as well as after demolding. The quality of the cast was assessed by comparing the measured density (mass and volume) with the nominal one. In addition, a Micro Computed Tomography (µCT) scan was carried out for test samples to determine defects in the RC such as blowholes, voids and cracks. This was conducted prior to the final design of AVES II, to recognize errors in the new manufacturing process. Two of these samples can be seen in Figure 13 and Figure 14.

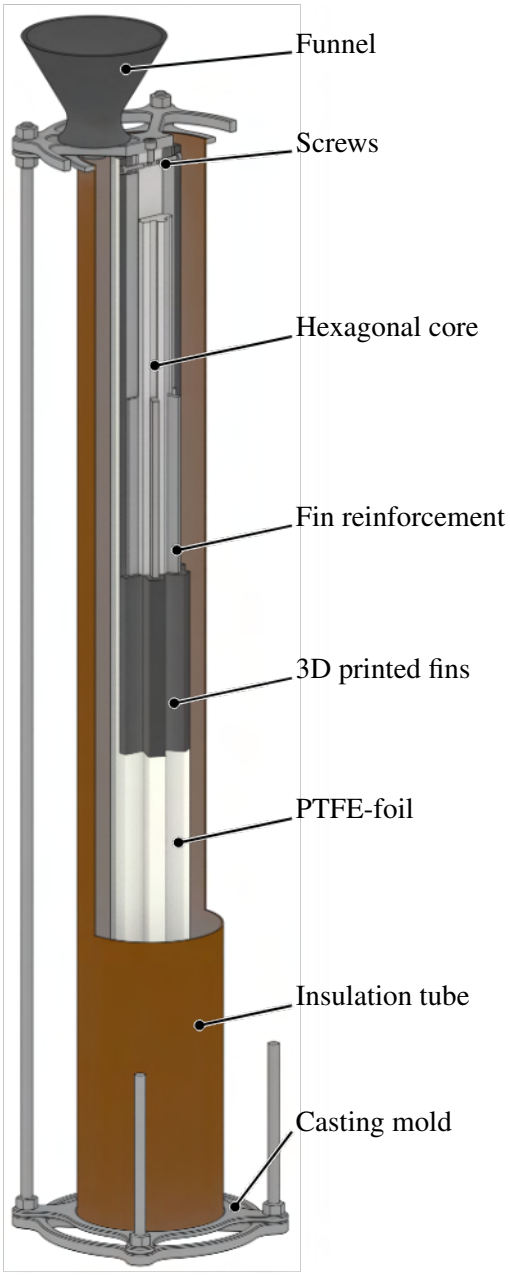

Figure 10: Assembled Castingmold

Figure 11: Meltingpot

Figure 12: Fuelgrain

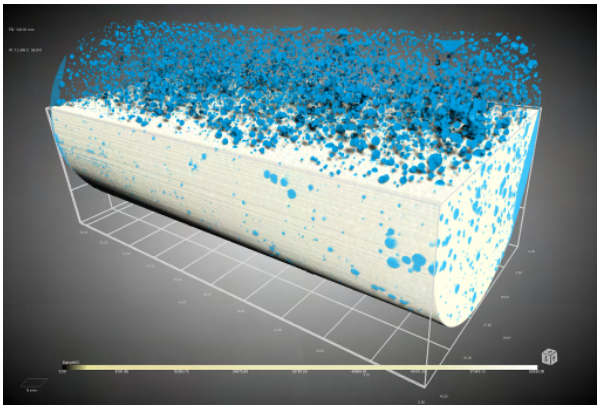

Figure 13: Visually assessed µCT Scan Sample 1, void voxel to total voxel ratio: 1.8 %

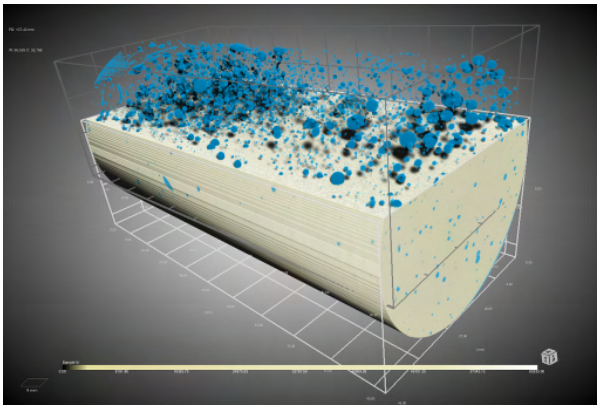

Figure 14: Visually assessed µCT Scan Sample 2, void voxel to total voxel ratio: 1.5 %

3.2.3. Ignition

The ignition of the booster is done with a so called Dome-Sprayer using a ignitor lift design for insertion.

The Dome-Sprayer consists of a 3D-printed hull, 53 mm long and 23 mm in diameter, filled with about 20 g of a pyrotechnic mixture. This mixture contains 60 % rocket candy made from 35 % sorbitol and 65 % KNO_3, 25 % calcium silicide and 15 % magnesium powder. The rocket candy acts both as a binder and a pressure generator, while the metal powders produce hot sparks for the ignition of the booster core. Through experimentation, the ratios were chosen such that the maximum amount of metal powder could be mixed into rocket candy, while maintaining a smooth, pliable mass as a result. Figure 15 shows both the 3D-printed hull with the lid of the Dome-Sprayer, as well as a hull filled with the pyrotechnic mixture. To increase the burn area in the ignitor (for short and intense ignition), a cross-shaped port was created with the help of a stamp. Figure 16 shows one of the ignitors during a test. The Dome-Sprayer itself is ignited by two redundant e-matches, inserted through dedicated holes in the lid.

Figure 15: left: hull and lid of the Dome-Sprayer in Computer Aided Design (CAD), right: hull filled with pyrotechnic mixture and lid with inserted e-matches

Figure 16: Dome-Sprayer during test firing. The length of the shot is approximately 130 cm.

For the insertion into the booster, the so called ignitor lift is used. It consists of a wooden plate with two holes and two thin wooden guiding rods glued into it. After two strings are guided through each of the holes, the plate including the strings and rods is mounted into the no combustion chamber of the booster, whereby the rods extend out of the nozzle. To insert the ignitor, the base of the Dome-Sprayer is fastened to one of the strings. Then the guiding tunnels are placed over the wooden rods. Pulling on the string subsequently lifts the ignitor up through the booster into the no - combustion chamber, to its predefined position. The second string serves as a redundancy, in case the first one is pulled out accidentally (e.g. when fastening the ignitor). Figure 7 shows the CAD drawing of the lift (without modeled guide rods) and the Dome-Sprayer.

3.2.4. Performance Analysis

From the experience with the motor of our first competition rocket, AVES, a strong dependence of the burn rate on the grain density is known. To account for this effect, a so-called void coefficient was included in the simulations for the booster performance, which basically modifies the burn rate of the propellant based on its the density [27]. For AVES II, a minimum requirement for the fuel grain density of 97 % was defined, leading to the requirement of 35 bar, as the maximum expected combustion pressure. However, an improvement in casting as described previously, made this precaution redundant, as densities around 99.9 % could be achieved consistently.

Testing

For the testing campaign of AVES II, a total of 12 hot-fire tests have been performed to this date. Five of them were conducted by reusing a shortened version of the combustion chamber (Cropped Combustion Chamber (CCC)) from last year's rocket AVES. The corresponding technical drawing and test reports can

be found in the Appendix G.3. The main goal of this campaign was to demonstrate the key features of the AVES II propulsion system, such as the finocyl core design, direct casting into the insulation and the new production process for the propellant. Following the positive results of these tests, the AVES II motor was hot-fired four times, however with a durable aluminum tube (not weight optimized), as the focus of these tests was the performance of the motor. Finally, the engine was fired in its final configuration two times horizontally and one time vertically at the all-on vertical hot-fire test (Appendix C.15). A summary of the full scale system tests of the AVES II propulsion system in a tabular manner, can be found in Table 4.

Table 4: summary of hot-fire results

Grain no.	max combustion pressure	total impulse	burntime	propellant mass
C1	21 bar	11 281 Ns	3 s	9525 g
C2	20 bar	11 317 Ns	3 s	9415 g
C3	20 bar	11 201 Ns	3 s	9400 g
C4	20 bar	10 759 Ns	3 s	9025 g
C5	17.5 bar	10 756 Ns	4 s	9480 g
C6	17.5 bar	11 007 Ns	4 s	9480 g
C7	16 bar	11 372 Ns	4 s	9500 g

Test setup

The hot-fires were conducted on our booster testbed, which is a horizontally arranged construction, equipped with different sensors and power supply. Following the philosophy “test as you fly, fly as you test”, we use our own SRAD hardware for the data acquisition unit, with the same 32-bit dual core ARM processor as in our rockets. A self developed, 8-input Analog-to-Digital Converter (ADC) card, with adjustable gain amplifiers is used to sample the data. Via a cable connection, the data is transmitted 100 m away, where the testbed is controlled and the data is logged with a self-developed software. Every hot-fire was conducted using two load cells, one pressure sensor and at least one thermocouple. A detailed description of the sensors used in the respective tests can be found in the detailed hot-fire reports in the Appendix C.3.

In Figure 17 the testbed can be seen during a hot-fire. The booster is mounted horizontally on linear guides, ensuring the whole thrust is transferred to the load cells. With the help of earth anchors and tension straps the setup is secured to the ground, ensuring no shifting of the testbed during firings.

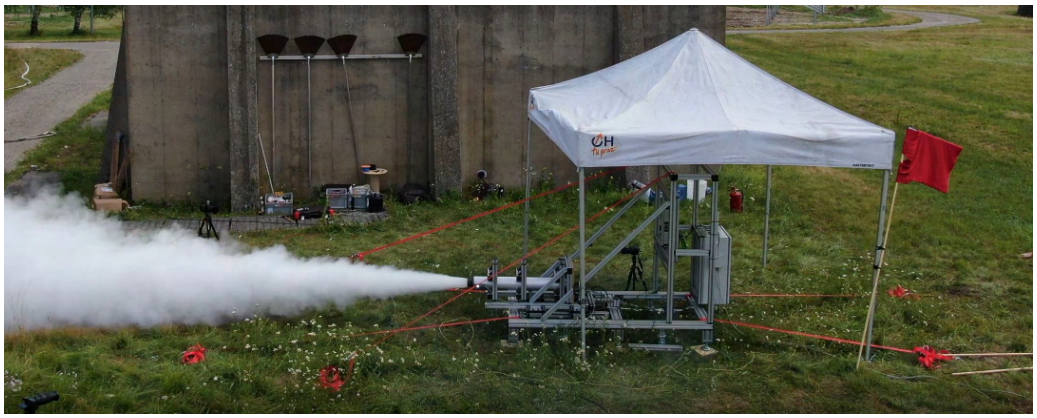

Figure 17: Testbed during a hot-fire test

Simulations

For the evaluation of the data collected in the hot-fire tests, a physics based, parametric regression scheme was employed. The SRAD python program Solid Rocket Simulation - Time Driven (SRS - TD) for this

is based on the formulas proposed by Nakka [15] and is consistent with other simulation programs such as “Meteor” [6], when given the same input. The main difference is, that the program allows a quasi 2D simulation, as it splits the grain into virtual segments along the axis. This enables the definition of a spatially and temporally variable burn rate. Thus, the inhomogeneous ignition or “flushing” (faster material erosion near the nozzle) of a fuel grain can be simulated by sequentially increasing or decreasing the burn rate at the respective positions. These individual burn rates can be collected in the form of a so called burn-rate-coefficient coefficient matrix, each entry representing a multiplicative factor for the non-corrected simulation.

The main findings of the simulations were:

- There was nearly no delay due to the ignition
- Some of the tests experienced significant flushing
- The combustion efficiency was quite low at $\eta \approx 60\,\%$, which reduced the measured pressure but not the total impulse, due to the high density of the unburned/partially burned products.

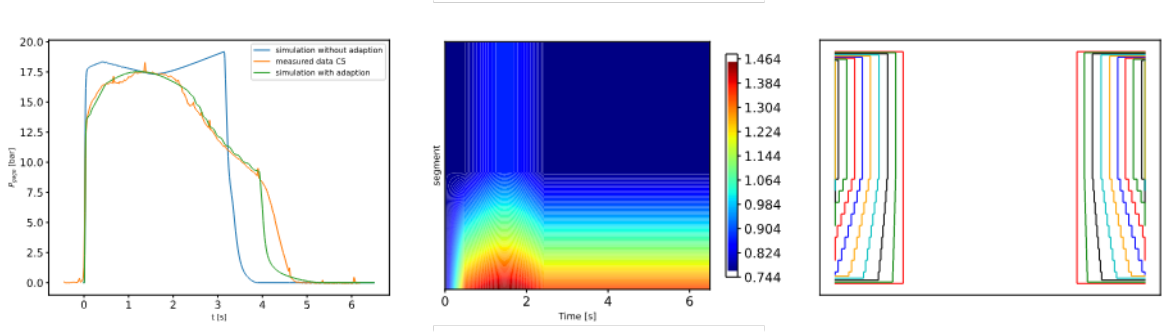

Figure 18: Example for the application of SRS - TD on the first test of the third hot-fire (C5).
Left: comparison of the simulation of the booster without adaption, with the use of virtual segments and the actual measured data. Middle: burn-rate-coefficient coefficient (brcc) matrix of the simulation. Right: contours of the burning surface over the duration of the burn. In the middle and the right picture the bottom side is towards the nozzle, and the top towards the bulkhead.

3.3. Aerostructure Subsystem

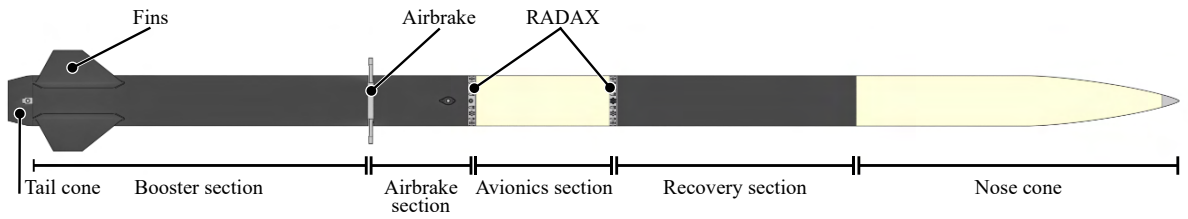

Figure 19: Overview of airframe sections

The airframe consists of six main sections. The nosecone section (NC-S), the recovery section (REC-S), the avionics section (AVI-S), the airbrake section (AIR-S), the booster section (PRO-S) and tailcone (TC). The sections are joined by two RADAX joints, the airbrake housing and the nose cone coupling tube (NC-CT). The main goals for the design for the aerostructure were:

- minimization of mass
- easy integration of the individual subsystems inside the rocket
- minimization of components

These goals were achieved by using a load bearing composite hull, thus eliminating inner load-bearing structures, by combining multiple tasks into single components. This was achieved by working closely with the other subsystem teams to determine integration possibilities, by using detailed analyses to determine airframe loads and using this data to optimize the topology of individual components and by using high performance material in conjunction with novel manufacturing methods.

3.3.1. Loadcases

To determine external as well as internal loads acting on the airframe, a python script was developed. Inputs including component properties (mass, CoG, MoI), interface points, scenarios (with different boundary conditions and different acting loads), rocket dynamics, aerodynamic forces from Computational Fluid Dynamics (CFD) simulations, external forces (parachute, handling), internal forces (booster thrust profile) are taken into account. Different load scenarios for various flight stages were defined:

- Handling
- Mounting (onto launch rail)
- On launch rail
- Flight
- Flight + Sidewind
- Flight + Airbrake
- Recovery Drogue Nosecone
- Recovery Drogue
- Recovery Main
- Landing

For each scenario, reaction forces at boundary conditions and internal forces in longitudinal direction were calculated in form of internal force diagrams for the whole rocket as well as individual interface loads. One of those diagrams ($N_x(x)$, $Q_y(x)$, $M_z(x)$) for the overall rocket and scenario "Flight + Sidewind" can be seen in Figure 20.

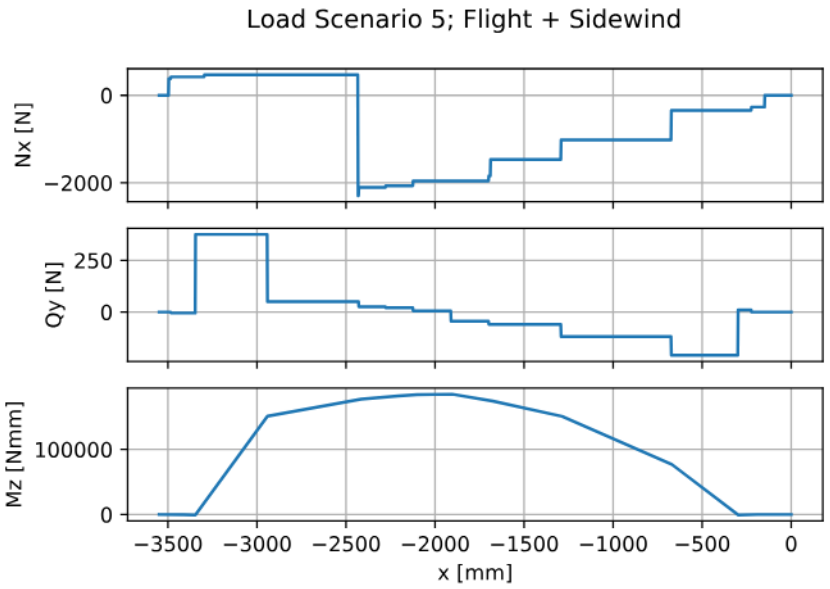

Figure 20: Scenario "Flight + Sidewind"($x = 0$ at NC tip)

Interfaces and loads per component are exported in NASTRAN syntax for an automatic import into our FEA program. The outputs were used for dimensioning the main structural parts. The loads for internal components were derived from the expected maximum accelerations. For a detailed analysis refer to the Appendix G.3.

3.3.2. Shell

The airframe consists of six main segments which are made from composite materials. Two main criteria had to be considered for the material selection and segment design:

Structural integrity
Structural analysis for the segments had to include considerations for tensile strength, buckling as well as the adhesive joints. The high tensile strength of CFRP and synthetic materials like PBO would allow a very thin outer hull. However, a certain thickness is required to provide stability and safety against buckling, since especially carbon fiber is significantly weaker across the fiber direction than along it.

RF-Transparency
Since carbon is conductive, it cannot be used for RF-transparent airframe sections. It was therefore decided to use a mix of Nextel 610 (CeFRP), glass and PBO reinforcements.
The first step in the design process was automating calculations for the classical laminate theory. The concept phase calculations were done with a rudimentary implementation in Microsoft Excel. During the design phase a Matlab script was written to further automate calculations. Results were verified by comparing data for identical layups of identical materials from our own script with data generated from Altair's ESAComp. The previously derived loadcases are combined into a tensor of the maximum stresses for all flight stages simultaneously. This allows for the most conservative results. The implementation of an optimizer using the Nelder-Mead-Algorithm led to the following layup and resulting maximum stress factors:

Table 5: Properties of airframe winded tubes

Section	Material	Lay-up [°]	Shell Thickness
NC-S	GFRP/CeFRP	(85,-10,10,-10,10,-10,10,-10)	1.21 mm
NC-CT	CFRP	(85,-10,10,-10,10,-10,10,-10)	1.56 mm
REC-S	CFRP	(85,-85,10,-10,10,-10,10,-10)	1.3 mm
AVI-S	GFRP/PBO/CeFRP	(85,-85,10,-10,10,-10,10,-10)	1.25 mm
AIR-S	CFRP	(85,-85,10,-10,10,-10,10,-10)	1.3 mm
PRO-S	CFRP	(85,-10,10,-10,10,-10,10,-10)	1.3 mm

Table 6: Stress Factors

Section	Stress factor	Criteria
NC-S	0.0199	Tsai-Wu
NC-CT	0.0084	Maximum-Stress
REC-S	0.0119	Maximum-Stress
AVI-S	0.1803	Tsai-Wu
AIR-S	0.0268	Tsai-Wu
PRO-S	0.0295	Tsai-Wu

3.3.3. Aerodynamics

The aerodynamic loads for the structural analysis of AVES II were calculated with the help of CFD simulations. In these simulations the rocket was simulated with the estimated Max Q conditions. The rocket was positioned in different pitch angles (up to 5°) and with the airbrake either retracted or fully extended. The forces on the rocket body were then calculated and used for structural analysis. To calculate all necessary loads roughly 5000 CPUh were needed.
To determine the aerodynamic characteristics of our rocket many CFD simulation were performed which accumulated roughly 20000 CPUh of simulation time. These simulations where mainly used to determine the drag coefficients of the rocket in the coast-phase which are used by the flight computer to predict the flight trajectory to accurately correct the apogee with the additional drag of the airbrake.

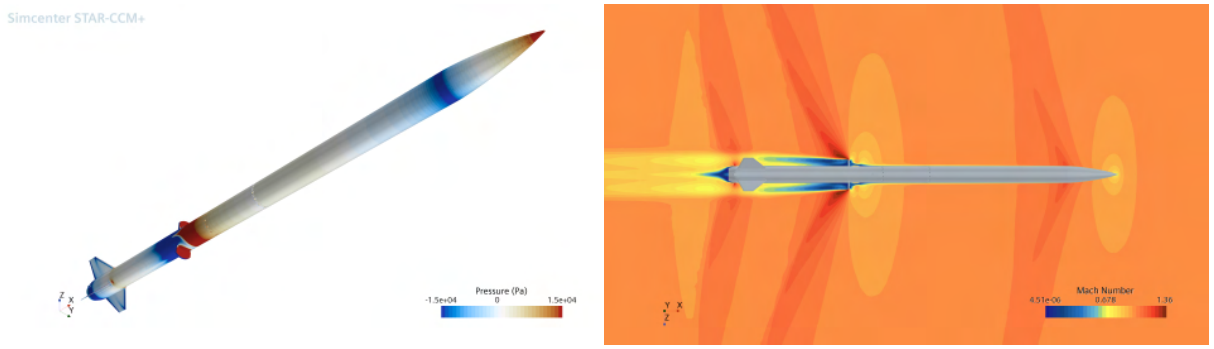

(a) Pressure contour plot

(b) Mach number contour plot

Figure 21: CFD simulation with the Airbrake fully extended at Maximum Dynamic Pressure (Max Q)

Nosecone

The nosecone was modeled after a special form of the LD-Haack Profile with $C = 0$, commonly called a von-Karman-Ogive. According to [5] this profile offers low drag over a Mach Range from 0 to 1.05, which matches the range encountered during a nominal flight of AVES II. The removable nosecone tip was manufactured from Aluminium to withstand aerodynamic forces and ensures a accurate aerodynamic profile, which would not be possible by fully filament-winding the NC-S.

$$\theta = \arccos\left(1 - \frac{2x}{L}\right) \qquad y = \frac{R}{\sqrt{\pi}}\sqrt{\theta - \frac{\sin 2\theta}{2} + C\sin^3(\theta)} \qquad C = 0 \tag{1}$$

Fins

The aerodynamic stability of AVES II is ensured by four trapezoidal fins with a thickness of 4 mm. The leading and trailing edge both have a double fillet and a blunted edge with a radius of 1.5 mm. The shape was chosen for aesthetic as well as manufacturing limitations. The sizing was optimized to achieve the required minimum takeoff stability of 1.5 body calibers at a maximum launch crosswind of 4 m/s in the design process. More details on stability margins can be found in Chapter 4.
The fins were manufactured with an integral flange from CFRP Prepreg [0/30/60/CORE/60/30/0] with a sidewall thickness of 0.6 mm and a Polyurethane (PU) foam core in a two-piece negative mold. The integrated flange is bonded to the booster section with epoxy adhesive (see test report **??**). The mass per fins could thus be lowered to under 75 g.
The mode shapes of the fins were simulated and used to calculate the critical speed at which fin flutter occurs (see Figure 22). The result is a critical speed of over 600 m/s which is significantly higher than the maximum speed encountered during a nominal flight.

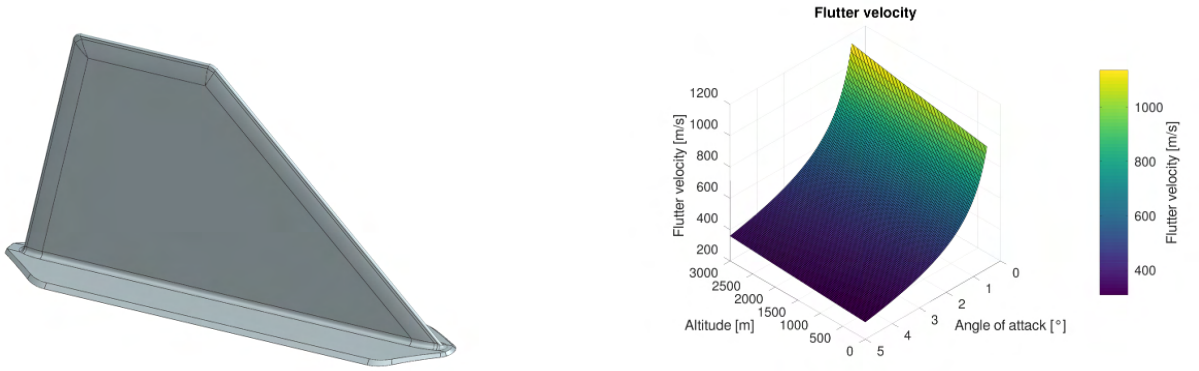

(a) Fin with integral flange

(b) Flutter velocity over altitude and AoA

Figure 22: Image of a fin and fin flutter velocity diagram

Tailcone

The tailcone is tangential to the booster tube and is tapered with an angle of 14°. This value was chosen as according to [12] this angle is the optimum for drag reduction in subsonic flow. The tailcone is made of carbon-fibre-reinforced-polymer (CFRP) with three layers of 0.2 mm carbon fiber cloth with an epoxy matrix. The tailcone itself only works as an aerodynamic cover with no load bearing purpose. It is mounted to the centering ring in the booster tube with four M3 screws.

Riblet Surface

Riblet foil is applied to the main airframe structure. It mimics the surface structure of shark skin with ridges along the rockets longitudinal axis. The foil interacts with near-wall turbulent structures to reduce the wall shear drag. In our case the total drag reduction across the flight regiment is about 2 %. [2]

3.3.4. Nosecone and Payload Structure

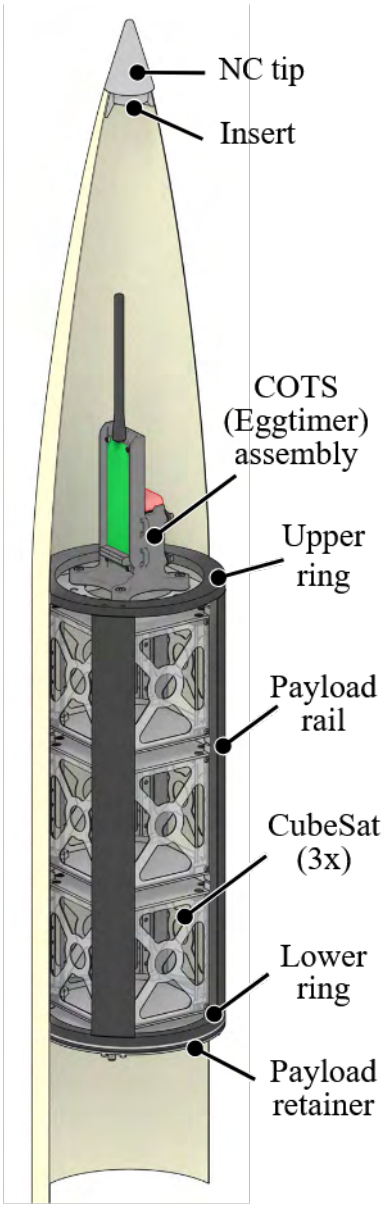

Figure 23: Sectional view of payload structure

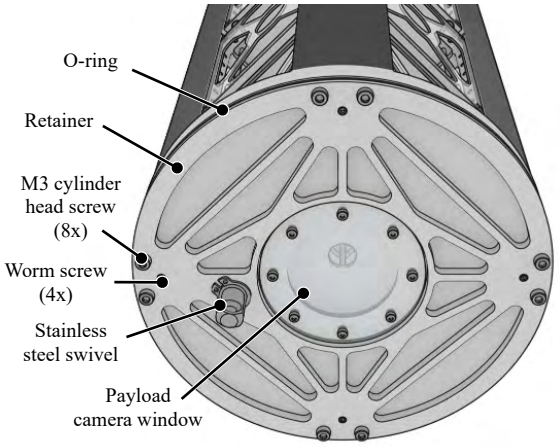

Figure 24: View Payload retainer

The Nosecone shell houses the 3U CubeSat payload as well as the COTS flightcomputer Eggtimer. The payloads and flightcomputer assembly is held by 4 rails made of 3D-printed PA 12 which allows for a straightforward integration of those subsystems by simply sliding them into the NC-S. Axially the loads are transferred to two load-bearing CFRP rings forward and aft of the payload stack. They are adhesively bonded to the shell with 3M©DP490 (see appendix subsection M). The payload retainer supports the payload stack in the back and is mounted with 8 M3 cylinder head screws to the lower CFRP ring. Furthermore, this plate seals the pressure chamber against the nosecone and features a stainless steel swivel, in order to connect the nosecone to the drogue chute and a Polycarbonate (PC) window to provide the lower CubeSat with a clear view of the deployment events. A FEA was performed in order to verify the plate can withstand the forces of the pressurization and to optimize the components mass (see appendix Figure G.3 for detailed calculations)

3.3.5. Coupling Tube and Pressure Chamber

The separable connection between NC-S and REC-S is realized with a CFRP coupling tube and is adhesively bonded to the REC-S. The nosecone is held in place by the tight fitting tube as well as 3 M2.5 nylon shear bolts. The pressure chamber formed by a CFRP plate in the aft and the payload retainer in front is pressurized by the first deployment system, which ejects the nosecone at apogee. The plate is held axially by an aluminium ring bonded into the coupling tube, which also holds the pneumatic tubing connecting the chamber to the first deployment (for calculations see appendix G.3). Due to the pressure and the undefined load path from NC-S to the coupling tube the wall thickness of the coupling was increased from 1.2 mm to 1.5 mm.

3.3.6. RADAX

The individual airframe sections are rigidly joined by two RADAX joints. One joint connects REC-S and AVI-S and provides an internal mounting point for the recovery baseplate and the avionics stack. The other joint sits between the AVI-S and AIR-S and acts as the lower mounting point for avionics as well as the arming, PadCom connector and camera hardware. Mounting assemblies directly to the joints allows for a direct and short load path to the rest of the airframe and eliminated the need for additional mounting hardware.

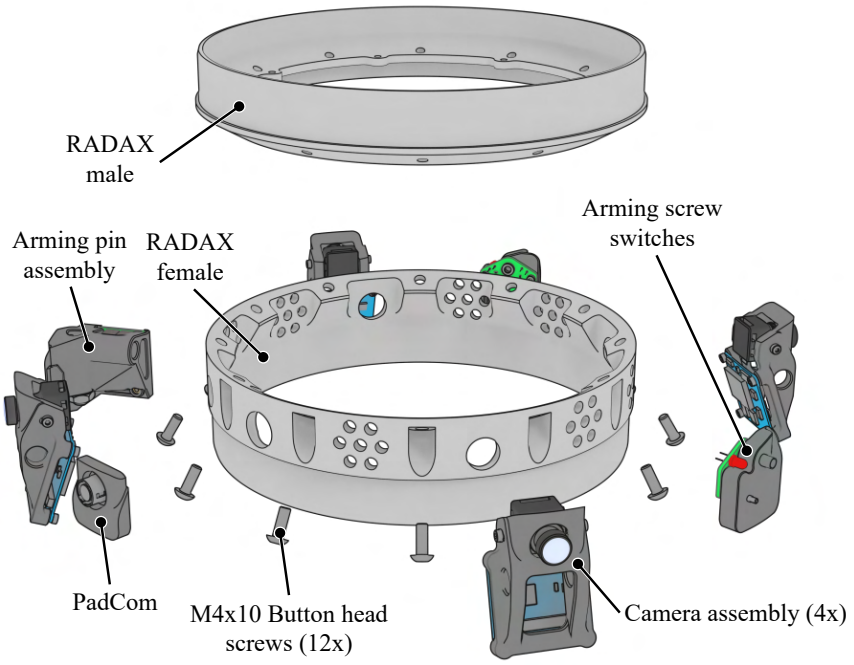

Figure 25: RADAX joint between AVI-S and AIR-S

Each joint is made of EN AW 2007 T4 and consists of a male and female half with a conical interface surface between them. The joint is preloaded with 12 M4x10 ISO 7380-1 button head screws, which completely eliminate play under load and give the joint very favorable stiffness characteristics. The stresses and bolt forces for all load cases were calculated with a multi-step FEA of the joint (see Figure A180) and were further used to validate the connection according to VDI-2230. Both halves of the joint are adhesively bonded to the respective composite hull with 3M©DP490 epoxy adhesive. The adhesive joint was analyzed according to the Volkersen methode (Schliekelmann modified) [10]. The detailed calculation can be found in the Appendix G.3.
The topology of the joint was further refined from last years design to reduce the weight of the joint. Unstressed material was removed in between the screw pockets and ventilation holes for avionics cooling were added. The mass of the halves was reduced to 144 g and 146 g respectively.

3.3.7. Airbrake

The airbrake system of AVES II consists of two plates which extend radially out of the rocket body. These plates create extra aerodynamic drag while extended and were optimized for maximum surface area given the number of plates. The plates are actuated by a servo motor which drives a central pinion that is connected to the racks on each plate.The plates are supported by two linear rails each which are bolted to the top airbrake housing. The design is inherently symmetrically even without power to the servo and therefore does not apply any pitch or yaw momentum. The location of the airbrake significantly behind

the Centre of Gravity (CoG) of the rocket ensures aerodynamic stability even when fully deployed. The plates are housed in between a base and a ceiling, which connect PRO-S and AIR-S to one another. Both of the airbrake housing parts are adhesively bonded to their respective carbon hull sections. The ceiling houses the linear guides and the servo mount and the base allows for cable routing to the booster sensor bay. In order to save weight and achieve the required stiffness a topology optimization of the plates was performed using the available volume limitations given by the housing and the aerodynamic forces from the CFD. The resulting free form was adapted for CNC milling and a FEA of the simplified design was performed. The servo motor together with the weight optimized plates can fully actuate the airbrake in under 200 ms.

Aerodynamic performance

The aerodynamic performance of the airbrake at Max Q was simulated to be 360 N per plate, meaning a total braking force of 720 N. The achievable apogee reduction was determined to be around 1000 m.

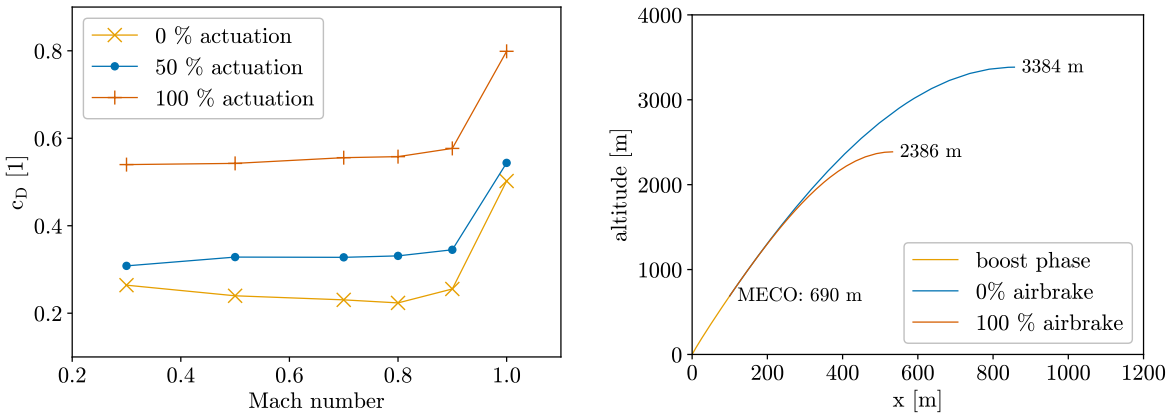

(a) Dependence of the drag coefficient c_D on the Mach number for different airbrake positions

(b) Effect of the airbrake on the apogee of the rocket

Figure 26: airbrake performance

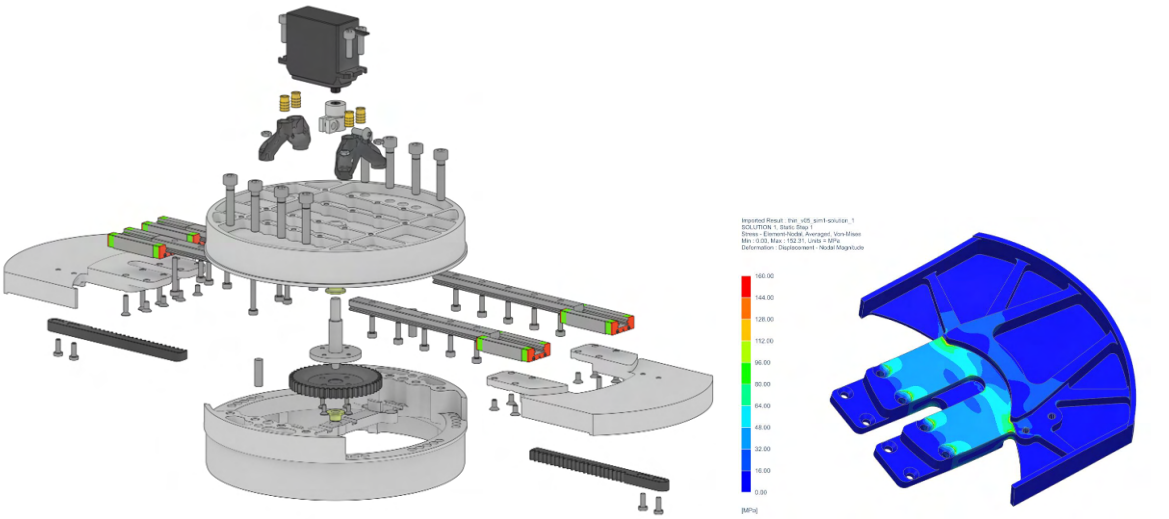

(a) Exploded view of airbrake assembly

(b) FEA results for the thin airbrake plate

Figure 27: Rendering of airbrake section and corresponding FEA of the thin plate

3.3.8. Thruststructure and Motorretention

The thrust structure of the rocket consists of the lower half of the airbrake, which acts as the front centering and transfers the thrust of the motor to the airframe. The airbrake lower half is connected with 8 cylinder head screws M5x25 ISO4762 to the airbrake upper half. At the lower part of the booster tube the motor is centered with a centering ring, additionally the booster insertion is simplified with omegaframes in the booster tube to prevent canting. The motor retention on the back of the rocket is realized with the railbutton and camera housing in the tailcone section as seen in Figure 28a. These two aluminium parts hold down the motor and are mounted to the centering ring in the PRO-S with two M3 screws each . To compensate for the thermal expansion of the motor casing an elastomer element is fitted between the lower motor retention and the motor. To protect the tailcone camera from the high temperatures during the burn, a heatshield was designed and tested. During the static hotfire test the temperature on the camera with the heatshield never exceeded 70 °C (without cooling air stream) see test report section C.3. The heatshield consists of a CFRP layer covered with aluminium tape for radiation shielding. The thrust structure and motor retention was tested at the all on vertical test. For detailed information see test report subsubsection C.15

3.3.9. Retractable Railbutton

The connection to the launchrail is realized with two retractable railbuttons. These railbuttons are spring loaded and retract after launch rail exit. The two launchrail connections are positioned in the area of the CoG and the rear of the rocket. The mounting of the front railbutton is an aluminium part which is joined to the carbon tube with epoxy adhesive and a forged carbon glide surface. The rear railbutton is a standalone anodized aluminum part which is mounted to the centering ring of the booster section.

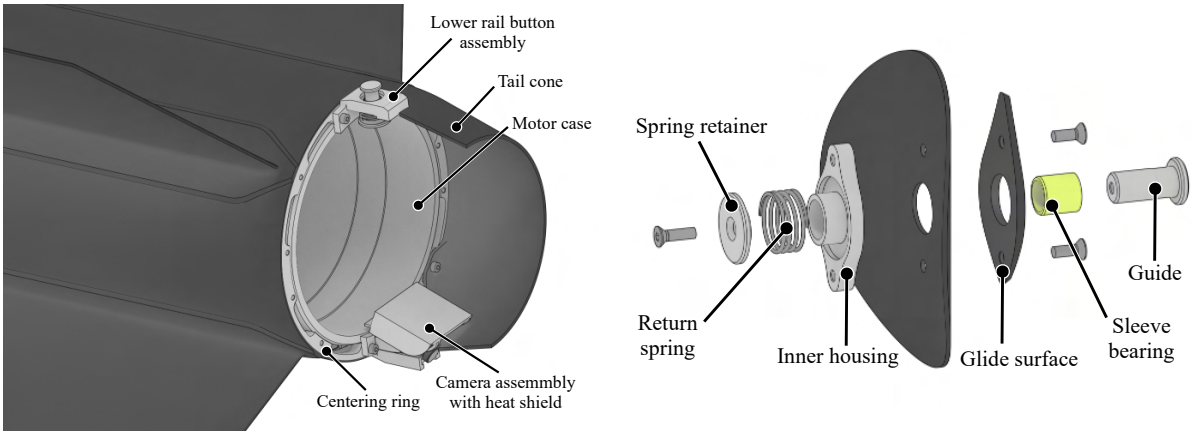

(a) Sectional view of tailcone assembly

(b) Exploded view of the front railbutton assembly

Figure 28: Rendering of tailcone section and front railbutton

3.4. Recovery Subsystem

The recovery subsystem consists of three systems:

- First Deploment
- Second Deployment
- Parachutes and lines

At apogee, the first deployment is triggered, the nosecone separates from the rocket and the drogue parachute is released. The drogue parachute will stabilize the descent and at 450 m altitude the second deployment will deploy the main parachute. The main parachute will decrease the velocity to 5.6 m/s for a safe landing. All systems were tested multiple times and documented with videos and test reports. The first deployment, which includes the igniting of the Nitrocellulose (NC) powder and the release of the Ar-gas from the cartridge was tested with different starting conditions. Furthermore, tests on the second deployment, which includes both linear actuators at the same time and individually, ensure it works properly. The first and second deployment were tested with a combination of the fully loaded recovery area and fully loaded pressure chamber to make sure the shear bolts work reliably. The self-sewn parachutes were tested for tensile strength in various places. Additionally, drop tests were performed. Finally, we also evaluated the complete recovery system when built into the rocket. Starting from the force, the drogue parachute needs to pull out the main parachute, up until the tensile-test of the eyebolt-connection to the ground plate. All reports on the tests can be found in Appendix C.1, the calculations can be found in Appendix G.2. In the subsections below, the individual subsystems will be explained in more detail.

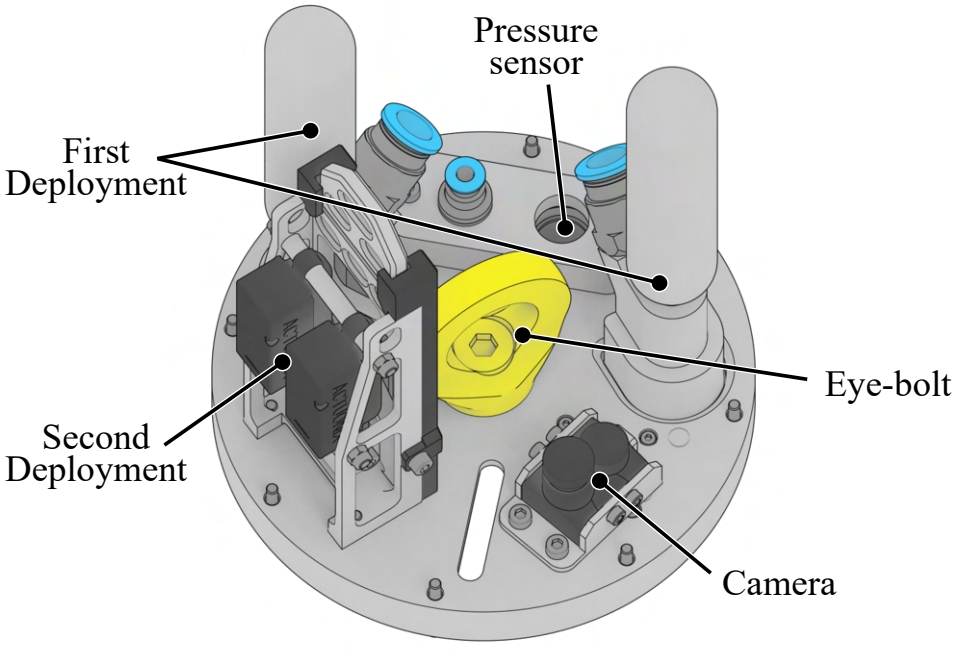

Figure 29: The Groundplate with all its components attached.

3.4.1. First Deployment

Operating procedure

The task of the first deployment is to separate the nosecone from the rocket at apogee (3000 m). For this purpose, a pressure chamber containing the drogue parachute is pressurized with argon gas. The over-pressure in the pressure chamber causes the shear pins, which are connecting the nosecone with the

rocket, to be sheared off. The three M2.5 polyamide shear pins can withstand a maximum over-pressure of 0.4 bar. In the pressure chamber we reach a pressure up to 4 bar minus the pressure losses of 0.2 bar. (see Appendix G.2)
Due to the height difference of 3000 m, a vent hole was provided in the pressure chamber for pressure equalization. The vent hole was accounted for in the calculations. (see section E.2) In the calculations, the pressure loss of 0.2 bar was calculated, which consists of the losses due to the height difference between the system and the pressure chamber, the deflection, the friction in the pneumatic line and the gas exhaust. The time for the gas outlet was determined during the tests and is 0.8 s on average. (see Appendix G.2)
After the separation process, both the nosecone and the remaining rocket are connected to the drogue parachute. The length of the lines ensures that the main body and the nosecone cannot collide. The kinetic energy of the nosecone and the pressure inside the parachute chamber then pulls out the drogue parachute.

Design
To pressurize the chamber, the opening mechanism was developed. Its idea is to open a capsule filled with argon gas after an electrical signal trigger the NC powder. The first deployment is mounted with two M3x10 screws on the ground-plate.A detailed overview of the design of the first deployment can be seen in figure Figure 30a and figure Figure 30b.

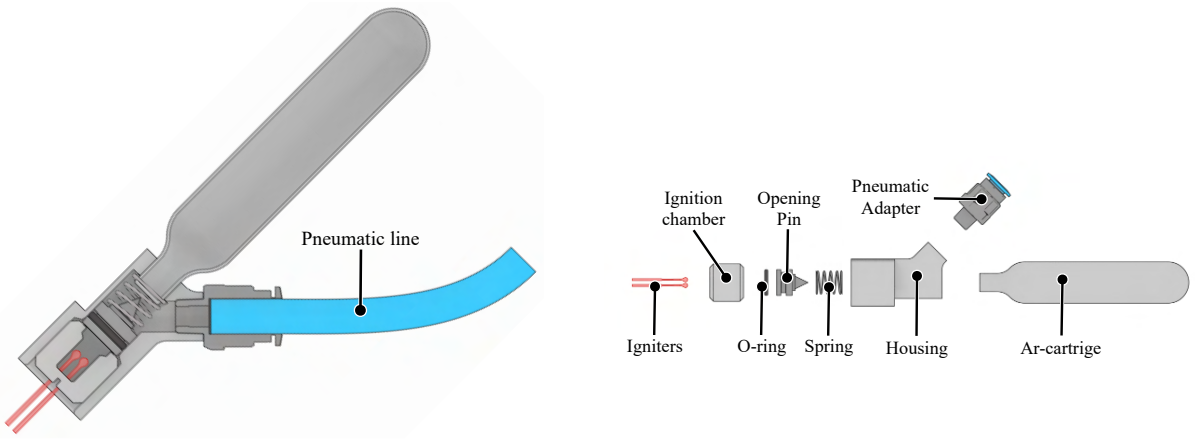

(a) Section of the First Deployment

(b) Explosion view of the First Deployment

Figure 30: First Deployment of the Recovery subsystem

Explanation of the mechanism
Two igniters trigger the NC powder at the same time. The expanding gas pushes the opening pin towards the argon cartridge. The tip of the pin pierces the membrane of the cartridge, venting the argon gas through the pneumatic tubing to the pressure chamber (see Figure 31). The high pressure shears off the pins, which are holding the nosecone in place and the nosecone with the drogue parachute will be ejected.

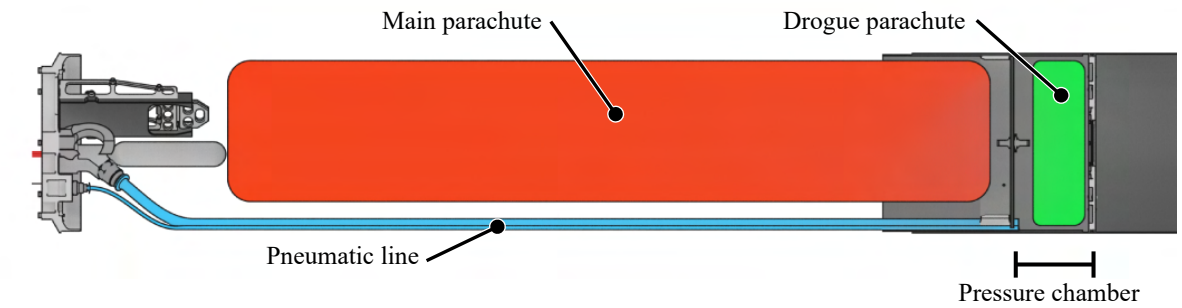

Figure 31: Overview of the Recovery section

Comparison between NC and black powder
The findings of the first tests are that we need less NC powder than black powder to get the same result. With black powder, a quantity of 0.15 g was necessary for a functioning system. By using NC powder, only 0.07 g of NC powder is required. Furthermore, the degree of contamination of the housing, the charge cup and the pin is lower when using NC-powder. We decided to use two-base NC powder to power our system. [19] [23]

Reasons for using Argon
For the system, unlike conventional systems, argon gas was used instead of CO_2 gas. In our system the cartridges are installed with the outlet facing downwards (Figure 30a), when using CO_2 there is a risk of CO_2 escaping in liquid phase,so there is a risk of it freezing during the gas discharge. Due to the lower freezing point of argon, this phenomenon cannot occur.

Redundancy
Two identical first deployments are built into the rocket to ensure that the separation process can still be guaranteed in the case of a failure of one system. In addition, two igniters were installed in each of the two systems. The electrical signals to trigger these mechanisms will activate both mechanisms at the same time, even though only one capsule is needed.

Pressure Sensors
Two piezoresistive sensors are used to measure the pressures in the recovery systems. One sensor measures the atmospheric pressure inside the recovery section during the flight while the other measures the pressure in the pressure chamber during the first deployment event. They are mounted in two bores inside the ground-plate and are held by the sensor cover featuring a simple opening for the atmospheric pressure as well as a pneumatic tube fitting for connecting the pneumatic tube leading to the pressure chamber.The implementation of the pressure sensors in the ground plate can be seen in sectional drawing Figure 32.

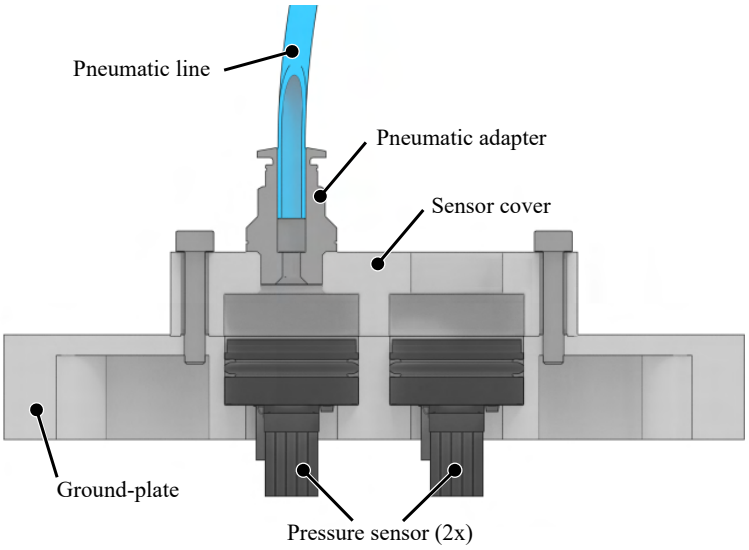

Figure 32: Built-in pressure sensors in the recovery ground-plate

3.4.2. Second Deployment

The objective of the second deployment system is to initiate the main deployment event and thus, releasing the main parachute. It is a system which relies purely on electrical power to operate. The load is released by two actuators and a rope, which uses the pulley-concept to distribute the force.

Design

The second deployment system can be split into two main parts, which are normally held together by a cord. The two pieces (*Groundplate Attachment* and *Top Mount*) can be seen in Figure 33.

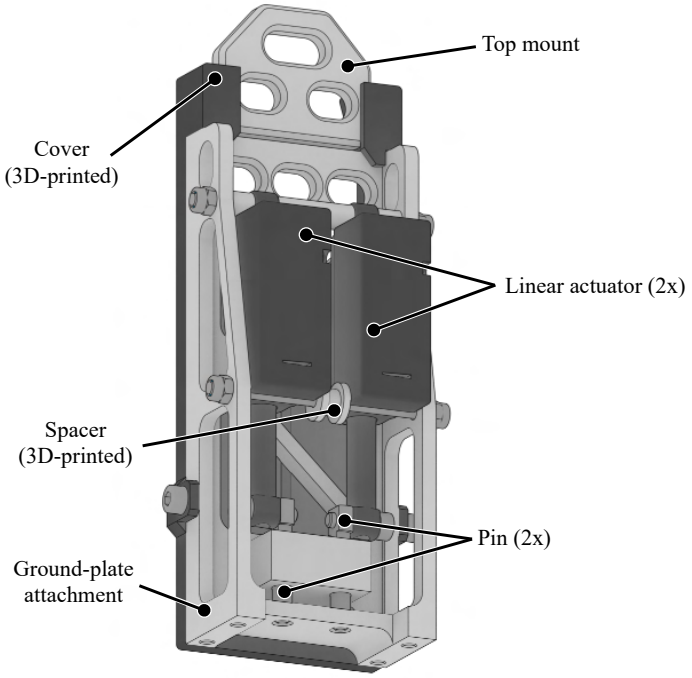

Figure 33: View of the Second Deployment in CAD, chord placement can be seen in Figure A15

The *Groundplate Attachment* is a piece of aluminum with structural cut-outs and holes on the top where the chord can be threaded through. There are two linear guides for aluminum pins, which will be retracted by the two linear actuators during the deployment. These pins hold the cord in place during ascend. The length of the guides was calculated (see Appendix G.2), to ensure, that the actuators have enough strength to pull them.
The *Top Mount* itself is an anodized piece of aluminium with three holes, as it can be seen in Figure 33. Two for the connection to the Groundplate Attachment by the cord, and the third one on the upper side for an elastic cord, which connects the Top Mount to the main parachute carabiner.
The two *linear actuators* from the manufacturer Actuonix, type *PQ12-100-6-S*, which means that they are operated on 6 volts and have a very low gear ratio of 100:1. These motors will pull the pins during the deployment.
An *endless cord* forms the connection between the two metal parts. This loop was self-strung and the material used comes from Paracord and is type 275. The cord itself is then threaded through the holes of the Groundplate Attachment and the Top Mount, and finally held in place by the pins of the linear actuators. When these actuators are activated, the pins retract to allow the cord to slip through the holes and so release the Top Mount from the Groundplate Attachment.
To hold on to the endless cord, a small *cotton thread* is tied to it. If the normal case occurs and both actuators open, then this thread stops the loop falling out of the rocket. If only one of them opens, it snaps due to the force of the drogue cute, and the loop is still held back by the other actuator.
A *3D-printed cover* is mounted on the backside, covering the loop to prevent it from getting tangled or damaged (by other parts within the recovery tube), and keeping the Top Mount in place. Additionally, a cotton thread is attached to the Groundplate Attachment and the cord to keep the loop from falling out of the rocket after the second deployment event.

Operating Procedure
At 450 m above ground level, the second deployment system is triggered. Electrical signals force the SD-Pins of the linear actuators to retract from the Groundplate Attachment. This allows for the cord loop to unwrap itself from the holes of the Groundplate Attachment, as well as from the Top Mount. The parachute, which at this point is only held back by the second deployment, then gets pulled out by the drogue chute.

Redundancy
The redundancy and thus the opening of the system is ensured by triggering both linear actuator independently. Each motor is wired with its own cable to the rocket's two flight computers.
If, for any reason, one of the linear actuators fails, the other one will still release the loop, and it will unravel itself from the Top Mount to release the main parachute.

Data & Tests
The minimum pull force required, varied with the left and right actuator (as seen in Test No.66 in Appendix C.1). This was due to the lacing of the loop, where one side has a bit more friction than the other side.

Left actuator: 34N	Right actuator: 20N	Both actuators: 6N

With a margin of safety, the pulling force should not be less than 45N. Due to the fact, that the Rocket itself weighs about 23 kg, this force will easily be exceeded. The self-made loop holds a load of more than 1,1kN, which is about 20 times the load that we need. This was also tested in Test No.66, which can be found in Appendix C.1.

3.4.3. Parachutes and Lines

Design

The green Drogue parachute has a cross-shape, as seen in Figure 34a. This shape was chosen from the first windtunnel test No.12 (see in section C.2) because of its flight stability and drag compared to the other parachute types. The lines are connected to the parachute by loops, as seen in Figure 34c. To reduce the force on the 90 degree bend, ribbons were sewn in to strengthen that area (see Figure 34b). Another windtunnel test (see test No.11 in Appendix C.2) verified the rating of the material used for the Drogue. In this test, the Drogue was ejected from the test stand into various wind speeds (15 m/s, 20 m/s, 25 m/s, 30 m/s). At opening of the Drogue a velocity of 19 m/s was calculated, therefore the windtunnel test verified the material used in the drogue. The drag coefficient was also estimated, as documented in test No.11, and with the uncertainty of the measurement, a c_W between 3 and 4 was chosen. With this uncertainty, two drogues were manufactured. With $c_w = 3$ and a side-length of 54 cm and $c_w = 4$ and a side-length of 46 cm the terminal velocity is around 24 m/s from equation (16) with $m = 23\text{kg}$, $\rho = 0.909\text{kg/m}^3$. When high wind speeds are observed on the launch day, the smaller drogue will be chosen to reduce drifts. Equation (18) shows, that with the Drogue a shock force of 114N can be expected, where instant opening is assumed, see Test No.72 in section C.2.

(a) Cross shape of the Drogue.

(b) Small black ribbons are sewed on the bend to sustain the loads.

(c) Lashes where the lines are connected to the parachute.

Figure 34: Drogue design

The red and white elliptical main parachute has ten gores and 20 lines are symmetrically connected through V-shaped lashes (see Figure 35a and Figure 35b). The diameter is 3.5 m and the apex hole is 20 % of the diameter, 70 cm. The drag-coefficient was estimated from drop-tests (see Test No.64 in section C.2) to 1.4. The terminal velocity was calculated with equation (16) and $m = 23\text{kg}$, $\rho = 1.1\text{kg/m}^3$

and yields velocities of 5.6 m/s. The opening time of the main parachute is not instant and therefore a different approach was used to calculate the opening loads. With equation (21) the maximum opening load is 633N with a $c_w = 0.9$ and 983N with $c_w = 2$. The materials used in the Main were tested in tention tests No.63 in Appendix C.2 where the safety factors were calculated.

(a) Shape of the main parachute.

(b) V-Lashes where the lines are connected to the parachute.

Figure 35: Main parachute design

The main parachute is stored in a deployment bag, where all the parachute lines are stored on the side in elastic loops (see Figure 36a). In order to prevent entanglement of any kind, a semi-removable cover was added, which is sewed onto the bag on one side, and loop fastener was added on the other side (see Figure 36b). Pull-out tests were conducted and were all successful (see test Test No.10 in Appendix C.2). The packing time of the main parachute, including the lines, is around 15 minutes.

(a) Folded parachute is already packed and the lines are stored on the outside.

(b) Deployment bag sealed on the edges with velcro tape.

Figure 36: Deployment bag for the main parachute.

The lines connecting the parachute with the swivel links have a length of 1.5 times the diameter of the parachute. The 20 main lines are 5.25 m long and the drogue lines are 69 cm and 78 cm long. The drogue shock-cord is 3m and the main shock cord is 7 m long. A detailed diagram of all lines and their lengths can be seen in Figure 37. The swivels at the end of the parachutes are rotating swivel that also move while under load. A M8 rotatable ringbolt is attached on the groundplate. The connecting point onto the nosecone is also rotating under loads. To prevent shearing from the air-frame on the main shockcord, a 10 cm long patch is taped over the line.

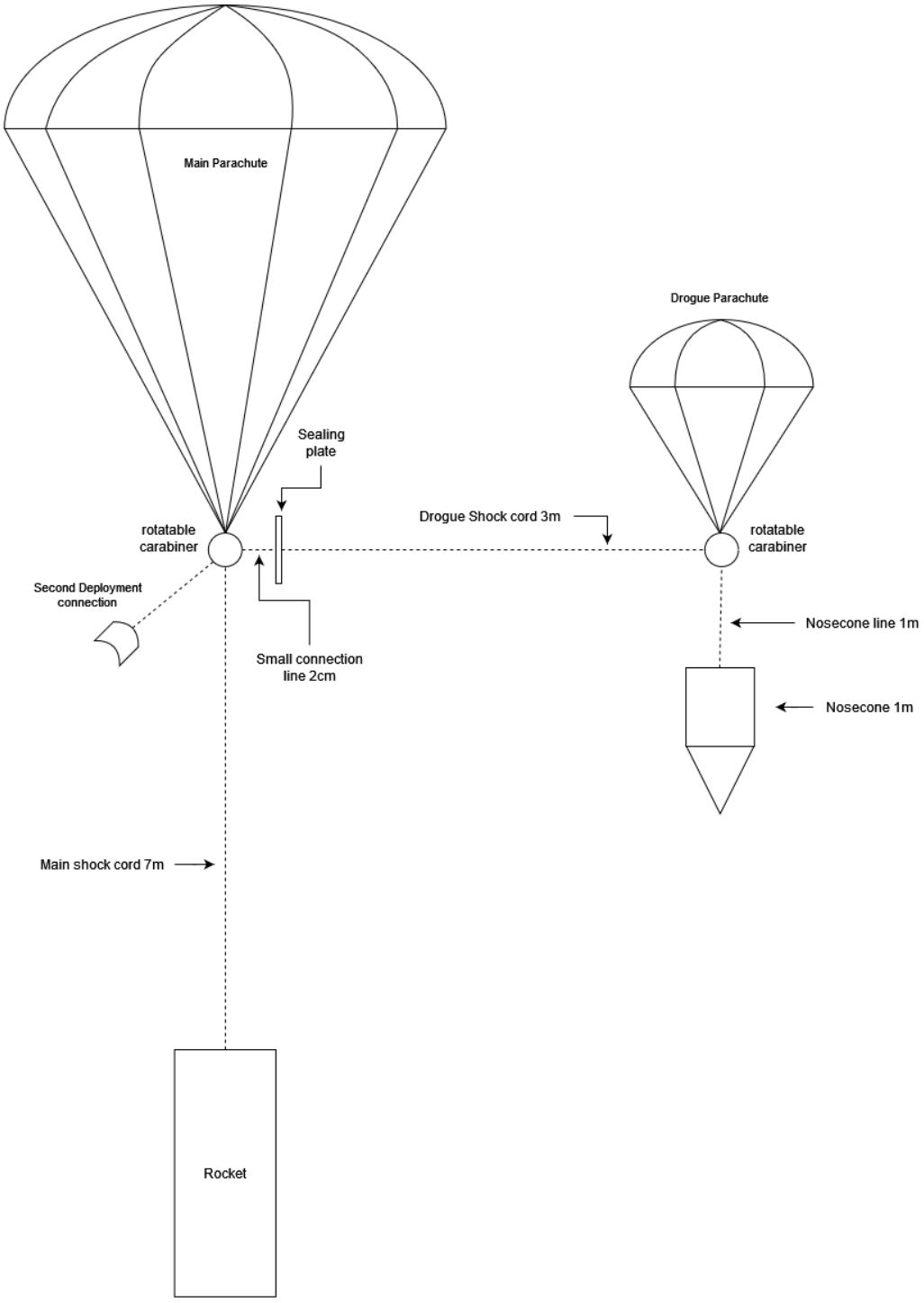

Figure 37: Line management between nosecone-drogue-main-rocket

3.5. Avionics Subsystem

The avionics of our system consist of multiple subsystems. The requirements of these systems are:

- Logging sensor data
- Triggering recovery events
- Controlling the Airbrake
- Recording and storing camera footage

} SRAD Flightcomputer

- Sending sensor data to the groundstation
- Visualizing sensor data on groundstation
- Remote communication with Flightcomputer

} Telemetry

- Remote booster ignition

} Ignition

In order to fulfill these requirements, we have designed multiple systems that are implemented on custom Printed Circuit Boards (PCBs). We divide these systems into our SRAD Flightcomputer, the telemetry and the ignition system. The SRAD Flightcomputer handles all events such as recovery and the Airbrake as well as gathering sensor data. For redundancy we chose to use the Altimax G4 from Rocketronics [20]. This COTS Flightcomputer ensures a redundant recovery deployment, in case our SRAD Flightcomputer fails and provides redundant altitude data. The telemetry system is responsible for sending the gathered sensor data from the Flightcomputer to the ground station as well as receiving the remote abort signal in case of an emergency. The groundstation is capable of visualizing the received sensor data in real time. It also provides all physical interfaces needed for mission control during a launch operation including the ignition control. To be able to ignite the booster remotely we also developed a Padbox that gets placed next to the launch pad and communicates with the groundstation. A overview of all components and their interactions can be seen in Figure 4.

3.5.1. SRAD Flightcomputer

The SRAD flightcomputer for AVES II is the successor to last years AVES flightcomputer. This years flightcomputer was developed under the premise of high reliability and robustness. The goal is to ensure a successful recovery and gather as much sensor data as possible for post-flight analysis. Therefore many sensors, of which most are redundant, are built into the rocket and get processed by the flightcomputer.

Hardware

The flightcomputer uses the dual core STM32H745ZI [25] Micro Controller Unit (MCU) with one Advanced RISC Machines (ARM) Cortex-M4 core and one ARM Cortex-M7 core, which are using a clock speed of 240 MHz and 480 MHz respectively. On the same PCB as the MCU, the main PCB which is depicted in Figure 38, four different sensors are placed twice each, for eight sensors in total: two BMP390 [4] barometers, two MS5607 [26] barometers, two BMI088 [3] Inertial Measurement Units (IMUs) and two H3LIS331DL [24] high g accelerometers. The two SAM-M8Q [28] Global Navigation Satellite System (GNSS) antennas are located on opposing sides of the avionics stack with their own ground plate PCB, to allow for optimal reception, no matter how the rocket is oriented. The flightcomputer uses two Secure Digital (SD)-cards to save all recorded data redundantly in addition to the internal flash storage, that is used for storing the data during flight.

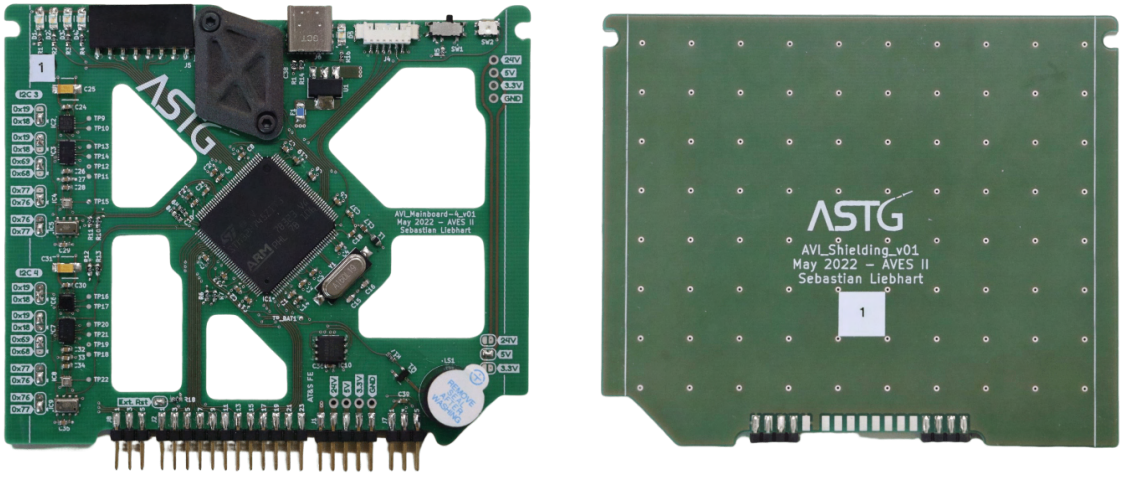

(a) Main PCB (b) Shielding

Figure 38: Flightcomputer Main PCB and Shielding PCB

Peripherals

In addition to the recovery electronics, the flightcomputer is connected to multiple peripherals, which are located outside of the avionics section. This includes the propulsion sensorbay (see Section 3.2.1), the recovery pressure sensors (see Section 3.4.1), multiple cameras (see Section 3.5.3), the airbrake (see Section 3.3.7) and the PadCom cable connector (see Section 3.5.3).

Software

The flightcomputer runs our own SRAD Real Time Operating System (RTOS) called RavenOS, which is based on SmartOS [21]. The use of an RTOS allows for multiple concurrent tasks that can interleave each other, which in turn allows our flightcomputer to do a multitude of jobs simultaneously. These jobs include, but are not limited to, reading sensor data from different sources, filter and process that data, communicate with the telemetry system and pad connection, control the airbrake, cooling fan and cameras, log all actions and data and of course trigger the recovery events. A detailed software diagram, depicting all the tasks can be found in Appendix J.2.

Kalman Filter

A Kalman Filter is implemented for sensor fusion. The inputs are the values of two barometers and two IMUs, which provide height, acceleration and angular velocity data.
To obtain the state transition function employed by the Kalman Filter, the equations of motion of the rocket were utilized. The state vector of the Kalman Filter consists of a three-dimensional position vector as well as its corresponding velocity vector, followed by a three-dimensional angle vector and its derivative, the three angular velocities. These form the 12-element vector which is crucial for the next steps in data processing and control.

State Detection

In Figure 39, the block diagram for the state detection is depicted. The necessary values are obtained by deriving the height values produced by the Kalman Filter. Between the derivations, some moving average functions ensure that the velocity and acceleration data are smooth enough as to not trigger any false state transitions.
The complete diagram of the state machine can be found in Appendix J.1.

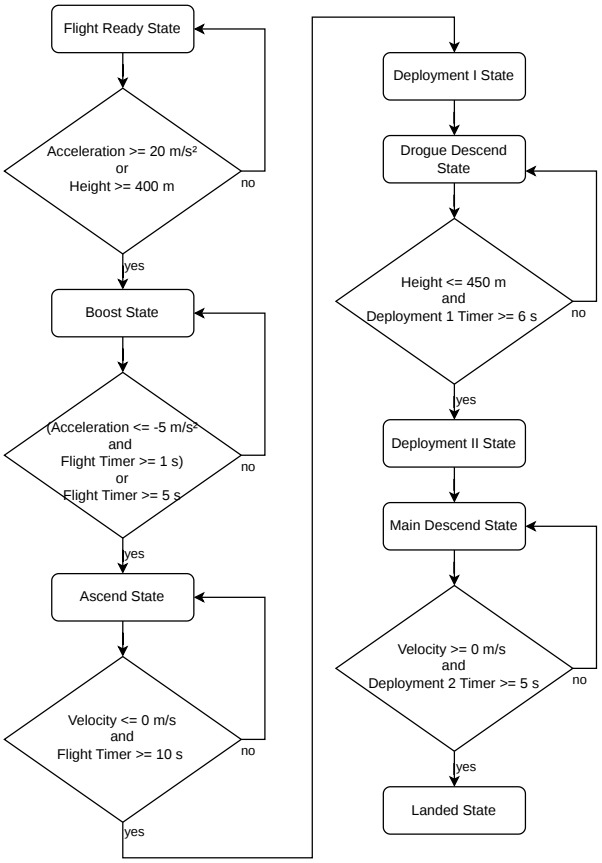

Figure 39: Automatic state detection diagram. Flight Timer represents the time since start detection (i.e start of Boost State), Deployment 1 Timer represents the time since apogee detection (i.e. the start of Deployment I State) and Deployment 2 Timer represents the time since deployment 2 height detection (i.e. start of Deployment II State).

Airbrake Control

In order to avoid having to prescribe a flight trajectory for the controller which drives the airbrakes, the flight parameters are converted into an estimate for the expected height at apogee. This constitutes the input for a discrete-time Proportional Integral (PI)-controller. Simulations show that this type of controller is promising as a robust and exact solution to meeting the mission's objective. In the calculation of the expected apogee, it is assumed that the actual airbrake position is held constant for the remainder of the flight, which in turn guarantees that there is a margin for both lowering and raising the height of apogee throughout the coast phase.

Figure 40 shows the graphs from the apogee height calculation and the control output, where a value of 1 corresponds to fully extended airbrakes. The controller is activated at booster burnout, which is visible in the control signal graph. The airbrakes are extended until the projected apogee reaches a value which is close to the desired altitude. Once this is achieved, the controller will account for uncertainties in the model and react if there is turbulence or other disturbances acting on the rocket.

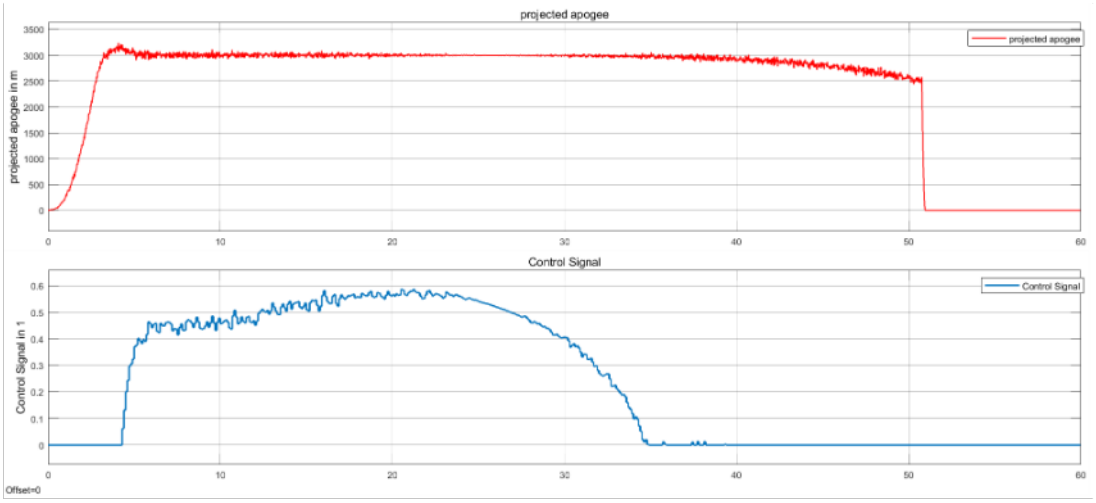

Figure 40: Projected Apogee height graph and corresponding Control Signal graph from Matlab Simulink.

Power Supply

Four batteries are used to supply power: one main 6s Lithium-Polymer (LiPo) battery for the SRAD systems, one 2s LiPo for the Commercial Off The Shelf (COTS), and two 2s LiPo batteries for each redundant set of recovery electronics. The different voltage levels needed for all the systems are created on the Power Supply Unit (PSU) PCB using a combination of switching and linear voltage regulators. This board also acts as the main interconnection for the other PCBs. Since no on-pad charging was implemented, a battery runtime of more than 8 h was targeted.

Arming

The arming system was designed with the goal to enable simple on-pad arming, but not relying on spring loaded mechanical switches as any failure-critical part. This was achieved using an arming-pin, which is removed on the pad to arm the recovery system, and two arming-screw-switches which can be armed beforehand, and are then only used to disarm the rocket on the pad or after recovery.

Recovery Electronics Circuit Diagram

Appendix K shows the complete recovery circuit, which extends over multiple PCBs that are shown as different blocks. Care was taken to separate the two redundant recovery electronics both physically and electrically wherever possible.

Blackbox

To ensure data can be recovered even in the event of a crash, one of the SD-cards is encased in 5 mm thick CFRP plates. The Blackbox is then mounted to the side of the Avionics Stack and connected to the Backplane/PSU PCB with a ribbon cable, that is directly soldered onto the SD-card. The mounting position can be seen in Figure 41.

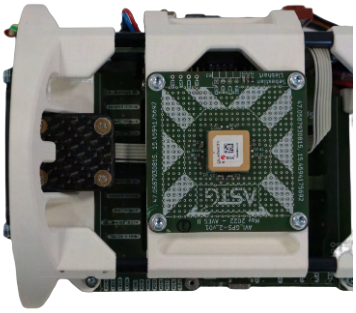

Figure 41: Mounting of the Blackbox at the bottom part of the Avionics Stack

3.5.2. Mounting Structure

For the integration of the avionics into the rocket we created a 3D-printed mounting structure that can be seen in Figure 42. The material used is ASA DuraPro [9] due to the improved thermal and mechanical properties compared to more conventionally printed materials. The bottom part of the structure houses the cooling fan, the blackbox, the COTS flightcomputer and the following PCBs: Mainboard, Backplane/PSU, GPS (2x), Telemetry, Shielding. The upper part servers as the mounting point for all LiPo batteries and the recovery interface. The whole structure is reinforced using eight carbon rods over the whole length. The patch-antennas are glued to two acrylic plates that are mounted on opposite sides.

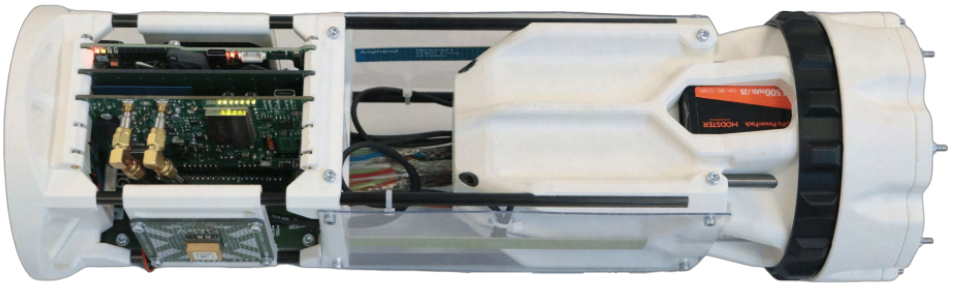

Figure 42: Assembled Avionics Stack

Recovery Interface

To allow for an easy and fast integration we developed a dedicated recovery interface that links the recovery deployment systems and sensors with the flightcomputer. The interface consists of a 3D-printed housing that attaches to the avionics mounting structure with a bayonet-like lock, and a lever-style connectors PCB (Figure 43a). It attaches to the bottom of the recovery groundplate, and allows for the connection of all recovery devices independent of our main flightcomputer. During integration the rest of the flightcomputer is secured to the recovery interface via the bayonet lock, and all necessary connections are made over the pin headers (Figure 43b).

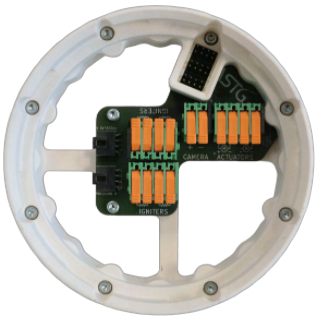

(a) Bottom

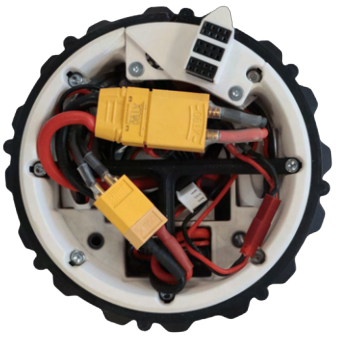

(b) Top view on mounting structure without recovery connector

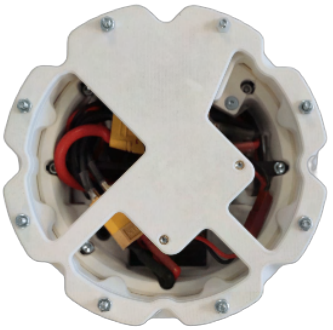

(c) Top view on mounting structure with recovery connector

Figure 43: Recovery Connector

Lower Interface

There are multiple systems in the lower part of the rocket that are connected to the flightcomputer. To allow for an easy and secure connection, multiple connectors are integrated into the bottom of the avionics mounting structure (Figure 44). These allow for connection to the propulsion sensor-bay, the

radial cameras in the lower RADAX joint, the tailcone camera, the airbrake servo motor, the recovery arming system and the PadCom connector.

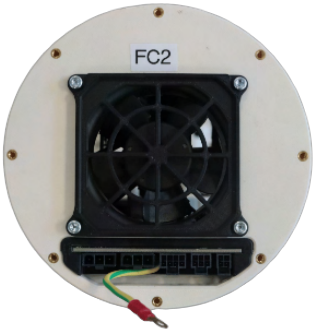

Figure 44: Bottom view on the mounting structure

Cooling

To prevent the electronic components in our system from overheating due to high power components and high temperatures we implemented an active cooling system. We realised this by integrating a fan into the bottom of the avionics mounting structure (Figure 44). It works by sucking in cool air trough the venting holes in the lower RADAX joint and pushing the hot air out of the venting holes in the top RADAX joint while passing all heat generating components. In order to get a good cooling performance we compared multiple designs using CFD simulation. We then took the best performing design and further optimized it leading to the results that can be seen in Figure 45. Everything combined the simulations took 500 CPUh to complete. The fan will be turned off during the ascend phase to avoid false barometric data from pressure changes.

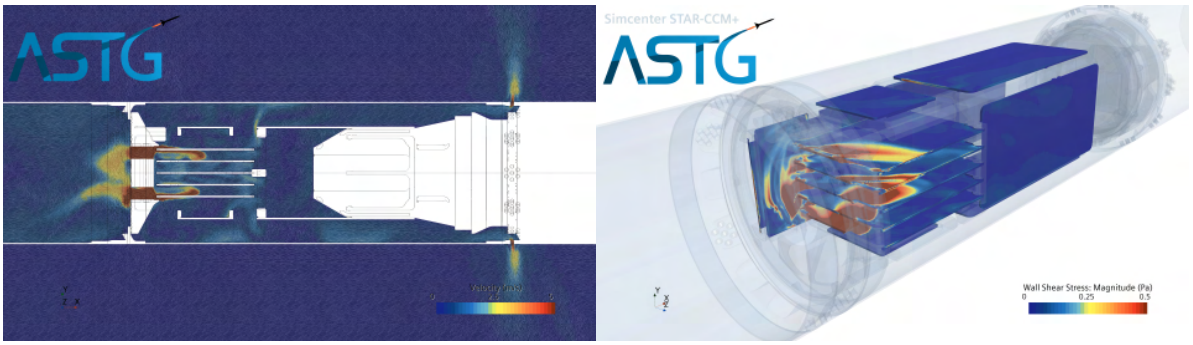

(a) Velocity (b) Wall Shear Stress

Figure 45: CFD Simulation of Fan Performance

3.5.3. Peripherals

PadCom

In order to communicate with the flightcomputer on the launchpad a cable can be connected to the rocket. Via this connection commands and parameters can be sent from a notebook to the flightcomputer and messages and data received in return. This is used to initialize the software and check the systems before launch, to ensure that all systems will perform nominal during flight, as well as arming the flightcomputer software. The connection can also be used to reset the flightcomputer without disassembling the rocket. A screenshot of the software is depicted in Figure 46. A diagram showing the state machine and all possible commands during each state can be found in Appendix J.1.

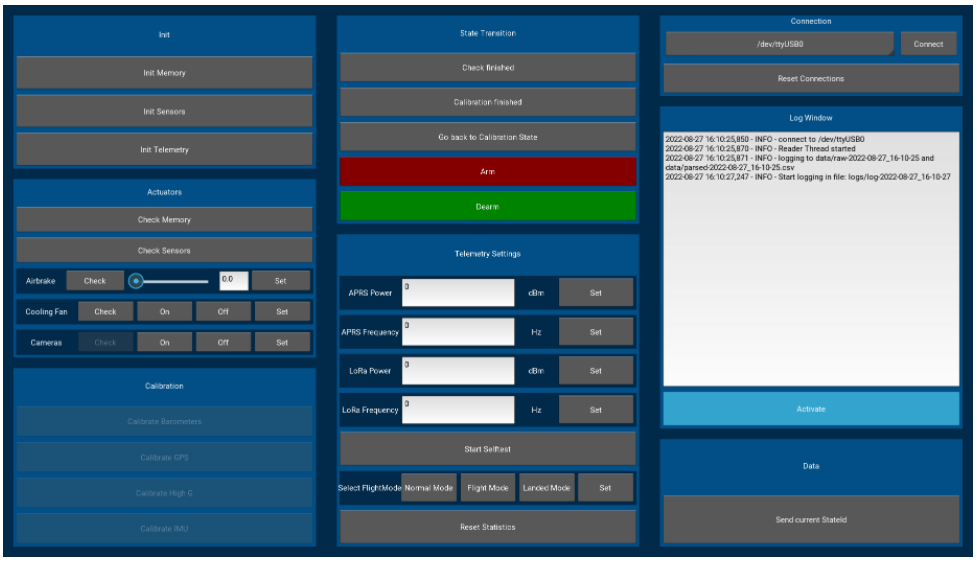

Figure 46: Software for initializing, checking and arming the flightcomputer

Cameras

AVES II houses a total of 6 cameras of 2 different types. We have one camera integrated into the recovery groundplate that films the second deployment event. For this we use the Runcam Hybrid 2 (Figure 47a) due to its high fps (1080p@120fps) capability. For the radial cameras located at the lower RADAX joint and the tailcone camera we use the Runcam Split 4 (Figure 47b) due to its smaller footprint and high resolution capability (4K@30fps/2.7K@60fps).

(a) Runcam Hybrid 2

(b) Runcam Split 4

Figure 47: Cameras used in the rocket

3.6. Telemetry Subsystem

3.6.1. Onboard

The telemetry subsystem onboard the rocket consists of one PCB, (Figure 48) and two omnidirectional dipole antennas. It receives data from the flightcomputer, over an Universal Asynchronous Receiver Transmitter (UART) interface, from the groundstation, over the Long Range (LoRa) link and transmits to the groundstation over the LoRa and the Automatic Packet Reporting System (APRS) link. All data transmitted between the groundstation, the telemetry system and the flightcomputer is using a custom packet format. Every packet has a type, which is used to route the packets between the systems.
The system uses a RP2040 [18] Dual-core ARM Cortex-M0+ processor controller. One core is used

to route all the data and to transfer it between interfaces. The second core is used to measure system parameters, to check for hardware faults and to control the power amplifier.

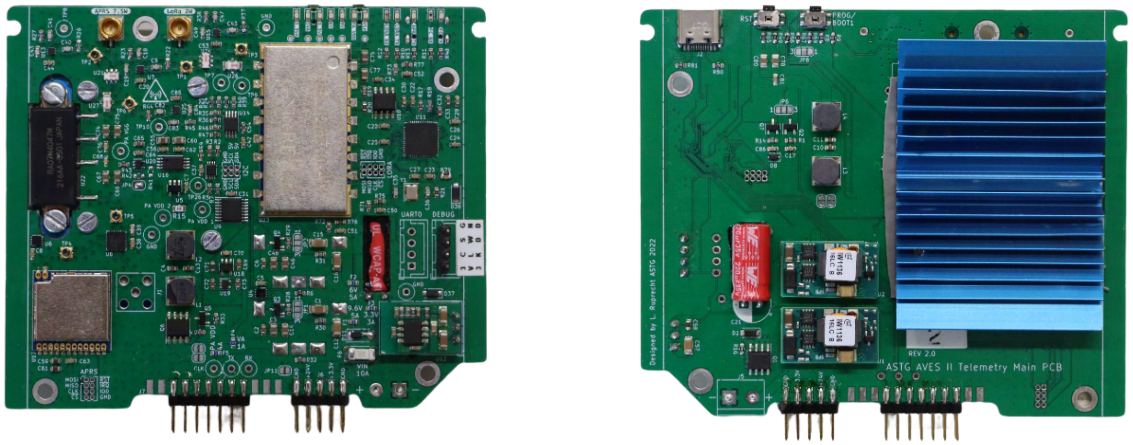

(a) Front (b) Back

Figure 48: Telemetry PCB

LoRa

The Long Range (LoRa) system is used in different ways depending on the stage of the flight. While the rocket is on the pad or flying, it is used as a bidirectional link to send commands to the rocket and to receive minimal parameters from the rocket at a low data rate. After the rocket lands, the modulation parameters of the system are changed, enabling transmission of position data at a very low data rate, but with greatly increased range. The system is based on a NiceRF LoRa1268F30 module [16] with a maximum output power of 2 W. The RF signal from the module is at first passed trough an 490 MHz lowpass filter. After the filter, the signal passes through a directional coupler to enable a power measurement of the transmitted and reflected signal.

APRS

The Automatic Packet Reporting System (APRS) system transmits data from the flightcomputer to the groundstation at a high data rate, about 40 kbps, using about 6 W of RF power. This system is based on a NiceRF RF4463PRO module [17], using the Si4463 [22] chip with Frequency-Shift Keying (FSK) modulation. The output signal from the module is passed to a the Mitsubishi RA07H4047M [13], an power amplifier Integrated Circuit (IC) rated at 7 W output power. After the amplifier, the signal is passed though a 490MHz low pass filter and the directional coupler.

Bi-directional Coupler

The telemetry board uses one bi-directional coupler for each of the wireless systems to measure the transmitted and reflected power. The coupler has two outputs in addition to the two ports, where the RF signal is passed through. One output provides an attenuated version of the signal traveling in the forward direction. The second output provides the same, but for the signal in the opposite direction. These signals are converted to a DC voltage, proportional to their power, using logarithmic amplifiers. The output voltages are then measured by an ADC and can be used to calculate the output and reflected power of the system. Using these results, the telemetry board can detect faults within the RF circuits of the board, damaged or defective antennas and antenna cables.

Antennas

The antennas that are used in the rocket are two PIOV004NRAA-100 from Amphenol MPC [1] due to their compact size. These are omni-directional antennas, therefore it is very important to match them to their surroundings. Given the used materials they aren't well matched (Voltage Standing Wave Ratio

(VSWR) < 4), so we had to correct that.
The major challenge while matching the antennas was keeping the surroundings constant, these are mounted right next to the batteries and cables which all influence the matching and efficiency. The tuning itself was achieved with different lengths of coaxial cable and an open stub that was soldered in parallel to the antenna. The shorted stub acts like a capacitor and compensates the inductive part of the antenna, therefore the imaginary part is getting smaller and we achieve a better return loss. With this tuning in place we measured an Standing Wave Ratio (SWR) of around 1.7 in the whole 70 cm band.

Figure 49: Onboard Antenna

COTS Altitude Logging and Tracking

For the official altitude logging and tracking we use the mandatory Eggtimer Quantum [8]. It is build into the nose cone section of the rocket using a 3D-printed mounting structure (section 3.3.4). It will not be used as redundant recovery electronics.

3.6.2. On ground

The stationary parts of the telemetry are housed in the groundstation that also provides power and protection from environmental conditions. A notebook can be connected to the groundstation using a USB Type-C connector to then save and visualize the received data. The other part consists of the two Yagi-Antennas to receive the incoming data which can be placed on the ground and be aligned using two tripods and self designed mounting hardware.

(a) Groundstation

(b) Yagi Antenna

Figure 50: Groundstation Setup

3.7. Ignition Subsystem

3.7.1. Hardware

The used hardware can be split into two parts, both contained in the Padbox and the groundstation. The first one are the PCBs (Figure 51) that are using similar parts to the telemetry system to lower development expenses, in this case the wireless (2 W) LoRa connection on 70 cm (433 MHz). The second one is the relay logic using industry grade process control components to provide the needed security in conjunction with the necessary keyswitches, buttons and lights to provide a user interface.

(a) Front (b) Back

Figure 51: Ignition PCB

3.7.2. Wired Connection

The Padbox and the groundstation provide both a wired and a wireless interface to ignite a rocket. Both interfaces use the same relay logic with lights, buttons, switches, keyswitches and relays, and the wireless interface uses the PCBs, capable of wireless communication and IO operations to transmit the different control signals, which are normally transmitted over the wires. It also needs to be noted that the key in the Padbox can only be removed in the off position to guarantee no ignition if that key is in possession of the ground personnel.

(a) Padbox (b) Spiral Antenna (c) Arming Light

Figure 52: Ignition Setup

3.7.3. Wireless Connection

In wireless operation, the groundstation PCB is the communication initiator and the PadBox only responds to status requests and action commands with the exception of error checking. This means the PadBox PCB can enter a error handling routine if it encounters any error, like wrong relay states or a connection timeout, where it then resets itself to a safe state. Both PCBs communicate errors to each other, so that both PCBs enter the error handling routine when anything off nominal happens and signal the error to the operator on the groundstation box.
The ignition procedure consists of three signals, first the communication test, second the arming signal and third the ignition signal. Each signal is initiated by a switch stroke from the operator and consists of two message exchanges, the readiness request with confirmation followed by the signal command with confirmation. In between signal exchanges, a polling routine is running, to detect connection losses.
For further information about the way the software works in the wireless configuration of the ignition system see the ignition state machine in Appendix J.3.

3.8. Payload Subsystem

AVES II is capable of carrying a 3U CubeSat payload to the target altitude of 3000 m. The payload compartment is located in the NC-S(more details in section subsubsection 3.3.4).
The payload itself consists of three 1U CubeSats designed and developed in cooperation with Polytechnic High Schools as well as one of our own team members as part of his Bachelor Thesis. The three CubeSats contain in three different payload projects and have a total mass of about 4 kg.

1. **CubeSat** Hawfinch (Jakob Faltisek / ASTG).
2. **CubeSat** Buffalo –REVD (Johannes Moser / HTL Neufelden, jm_space).
3. **CubeSat** Accipiter (HTL Pinkafeld).

More detailed information about the different Payload projects can be found in the Appendix G.3.

4. Mission Concept of Operations Overview

This section gives an overview of the AVES II Mission Concept of Operations (CONOPS). The main mission phases that describe the nominal behavior of all subsystems are summarized in Table 7. The flight phases along the trajectory can also be seen in Figure 53. Moreover, the main performance data including thrust curves, accelerations, velocities, aerodynamic stability, predicted apogee and more, are demonstrated in Figures 55, 57, 56 and Table 8. The measured thrust curves that are used for simulations are shown in Figure 54.

Table 7: Overall CONOPS at EuRoC 2022.: Mission phases and nominal operations timeline.

Mission/ Operational Phase	appr. Time (start)	Phase Start	Phase End	Aerostructure	Flight Computer	Telemetry and Groundstation	Propulsion	Recovery	Payload	Launch Pad Team	Recovery Team
Assembly	t = -2 h	Admission to preparation tent	Complete Assembly checklists and LRR pass	Rocket integration of assembled subsystems	Assemble AVI Subsystem, system checks	Setup, connection and system checks	Final preperations and visual inspection	Assemble/Prepare REC subsystem	Start-up and Health Checks	Launch Pad prep: setup Padbox, system checks, dry ignition tests	-
Booster Integration	t = -1.5 h	Transport of rocket from prep tent to pyro tent	Complete booster integration checklists	Install motor rentention and tailcone	-	-	Booster Integration (includes sensor connection)	-	-	-	-
Final Launch Pad Preparation	t = -1 h	Launch team carries rocket to launch pad	Rocket mounted on launch rail and AVI checks done	Install rocket on launch rail	Prepare FC for launch, system checks	Health Checks	-	-	-	Transport rocket to launch pad, mount rocket on launch rail, AVI checks	Recovery preparations
Recovery Arming	t = - 30 min	AVI Sotware arm	Hardware arming (arming pin removed)	-	Software arm, disconnect padcom and hardware arm of REC system	-	-	-	-	REC arming	-
Ignitor Insertion	t = - 30 min	Prepare ignitor lift for insertion	Ignitor connected to Padbox	-	-	-	Igniter insertion	-	-	Insert igniter	-
Ignititon Arming	t = -25 min	Padbox arm	Groundsation arm	-	-	Ignition arm	-	-	-	Arm ignition and walk back to mission control	-
Ignition	t = 0	Fire signal send to igniter	Propulsion system comes up to chamber pressure	-	-	Ignition, rocket com. and data downlink	-	-	-	-	-
Lift-off	t=+1 sec	First movements of rocket	Rocket is free of launch rail	-	-	Rocket com. and data downlink	-	-	-	-	-
Boost	t= +1.7 sec	Rocket is free of launch rail	Booster burnout	-	-	Rocket com. and data downlink, possible flight abort	-	-	-	-	-
Coast	t=+5.6 sec	Booster burnout	Apogee position	-	-		-	-	-	-	-
Apogee	t=+27 sec	Apogee position	Nosecone separation (1st REC deployment)	-	-	Rocket com. and data downlink	-	-	-	-	-
Drogue Descent	t=+27 sec	1st recovery deployment	2nd REC deployment	-	-		-	-	-	-	-
Main Descent	t=+120 sec	2nd recovery deployment	Landing/ Touchdown	-	-		-	-	-	-	-
Landed/ Recovery	t=+200 sec	Landing/Touchdown	Rocket recovered	-	Disarm REC system		-	-	-	-	Recover rocket (save handling procedures)
Disassembly	t=+2 h	Rocket recovered	Completed Post-Flight Review	Disassembly of rocket	Check batteries and secure data	Break down ground support equip.	-	Disassembly and check energetics (1st depl.)	Switch off and secure data	-	-

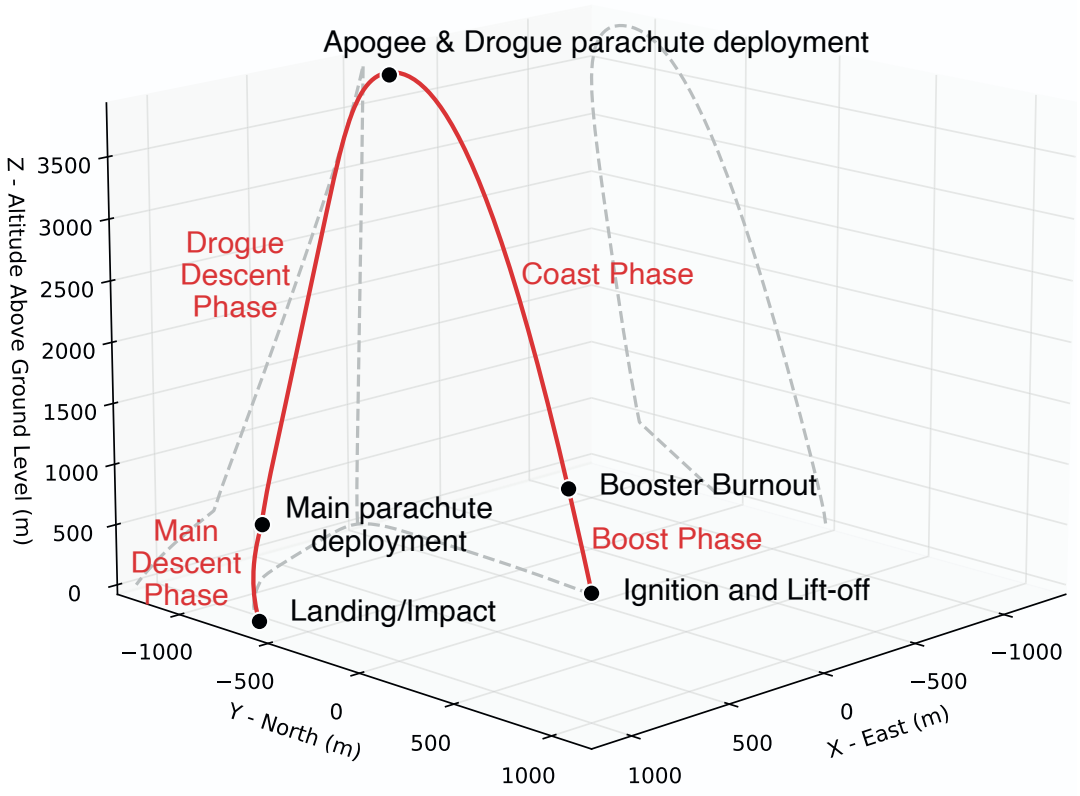

Figure 53: Exemplary flight trajectory simulation (RocketPy) with 2 m/s side wind from launch direction; The main mission phases (introduced in Table 7) are displayed; Note: In this simulation the airbrake was not actuated which usually happens in the coast phase, its effects are demonstrated in Figure 26.

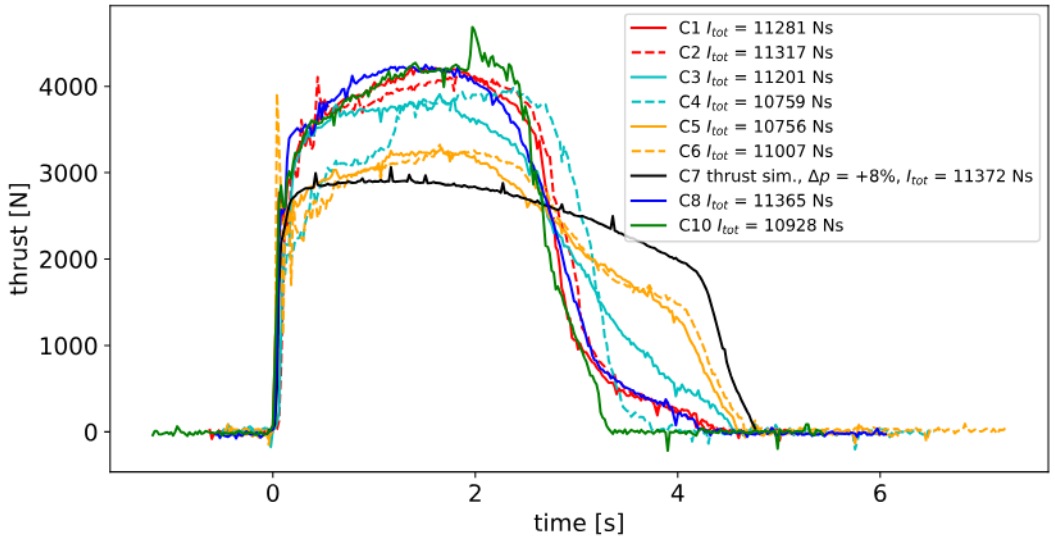

Figure 54: Measured thrust curves of the AVES II booster in consecutive order (see test protocols in Appenidx C.3).The color indicates Boosters cast in the same batch. While the shape of the curves vary from test to test, the total impulse remains at about 11 000 Ns; For flight simulations C5-C7 are mostly used; C7 represents a calculated thrust curve as only pressure was measured (All-up static hot-fire test see Appenidx C.15)

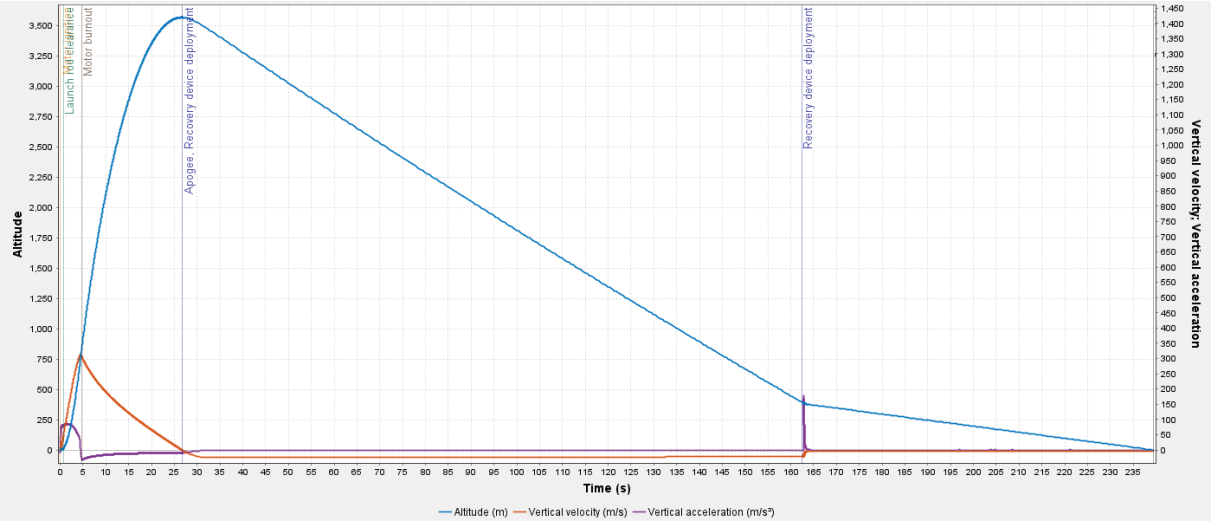

Figure 55: Open Rocket Simulation: altitude, vertical velocity and acceleration during flight (side wind: 2 m/s)

Table 8: Open Rocket simulation parameters for different side winds; drogue (dro) and main deployment (depl), decent (dec) velocities

side wind [m/s]	apogee [m]	v_{max} [m/s]	a_{max} [m/s^2]	$v_{dro.depl}$ [m/s]	a_{dro} [m/s^2]	$v_{dro.dec}$ [m/s]	a_{main} [m/s^2]	$v_{main.dec}$ [m/s]
2	3564	315	87.4	31	17	24	180	5
4	3539	315	87.4	31	17	24	180	5
6	3504	315	87.5	31	17	24	180	5
8	3480	315	87.5	31	17	24	180	5

All flight simulations were computed with different codes/software packages, namely: Open Rocket, RocketPy and Rasaero. While these simulations agree in most outputs, important quantities like the static stability margin differ by a factor of more than two, see Figure 56. We will take a closer look on the implementations and calculations of the codes. However, the criteria of having a static stability margin of > 1.5 cal is met in every simulation with a side wind of 2 m/s. Optionally, there is the possibility to add extra mass in the nose cone to increase stability. As an example, 2 kg of extra mass cause an increase of stability to 1.5 cal with a side wind of 8 m/s and a decrease in apogee of 200 meters.

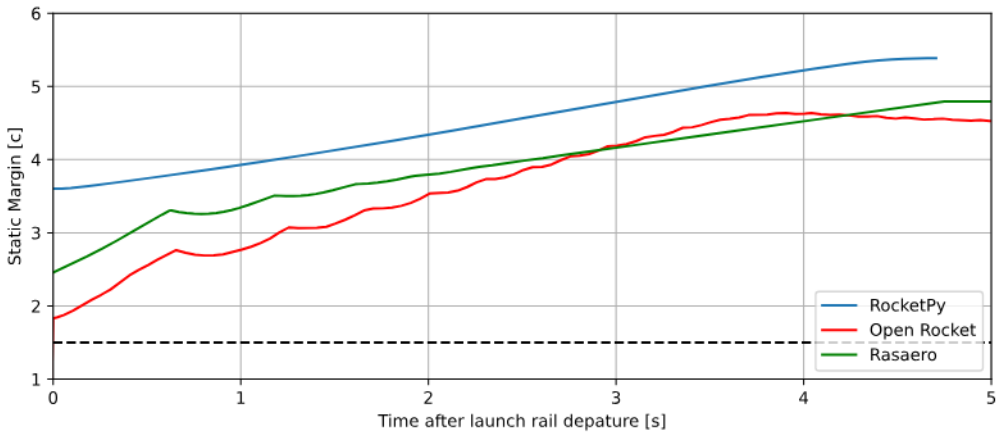

Figure 56: Stability margin from launch rail departure to booster burnout: Comparison of different simulation software (side wind: 2 m/s)

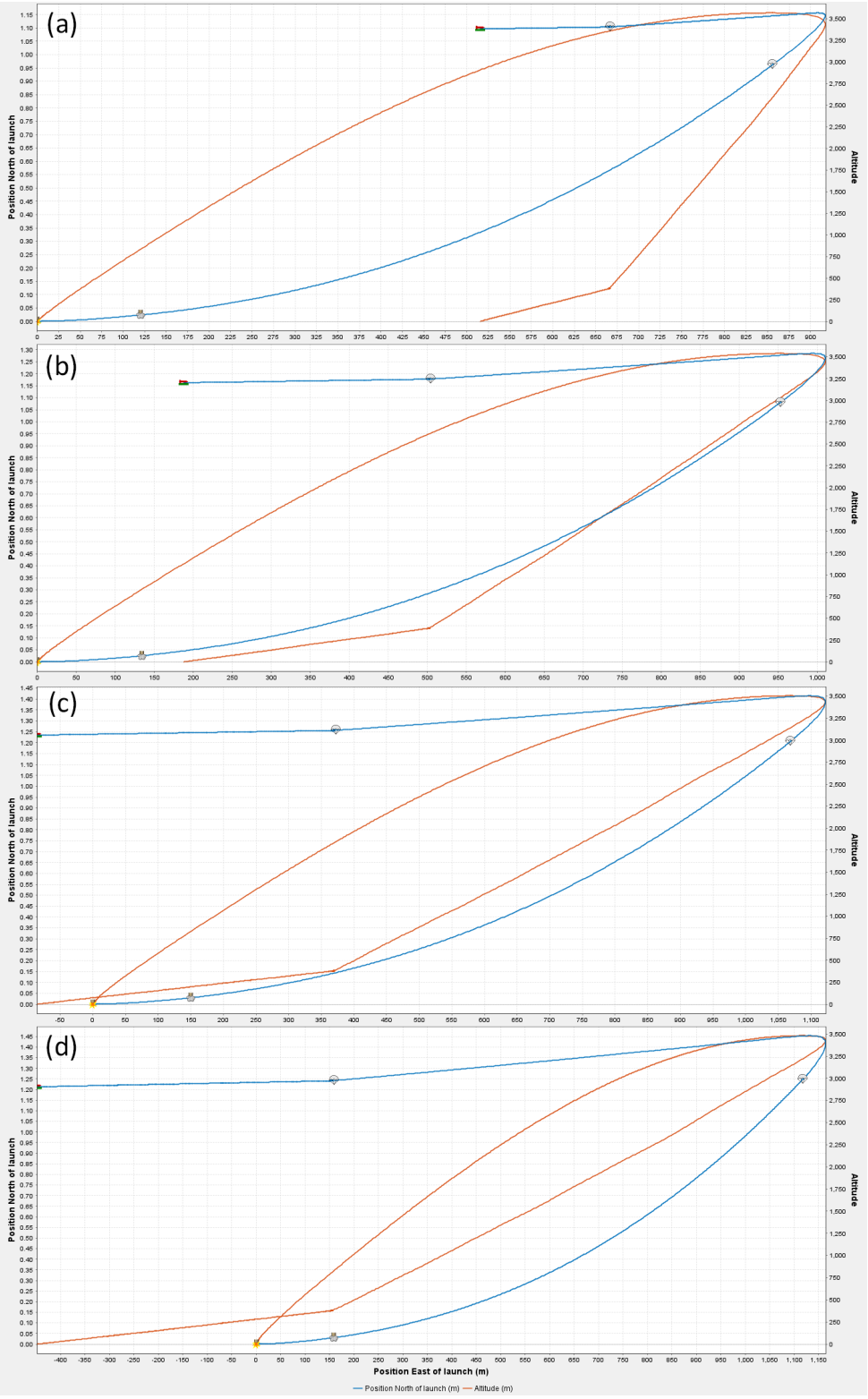

Figure 57: Open Rocket Simulation: Ground track and altitude during different side wind scenarios: (a) 2 m/s), (b) 4 m/s), (c) 6 m/s), (d) 8 m/s)

5. Conclusions and Outlook

This report deals with the design, development and manufacturing of AVES II the successor project of AVES and takes part in the S3 (SRAD solid, 3000 m) category of the EuRoC 2022. The rocket can be mainly separated into four domains, with their corresponding requirements/sections/tasks:

- **Aerostructure:** nosecone, Airbrakes, fins, tailcone, payload-enclosure, RADAX joints and shell
- **Avionics:** flightcomputer, telemetry and ignition
- **Propulsion:** solid rocket motor
- **Recovery:** parachute, first and second deployment systems

The payload consists of three CubeSats stacked on top of each other. Two CubeSats are outsourced to school projects and the third one contains a bachelor project of one of our team-members. This year we had some problems with our outsourced payloads. Two of the teams did not meet the agreed timetable and the overall project management was not as expected. Regarding our next project we might establish a CubeSat competition to select the school projects which will be flying with us.

One big achievement for this project is our SRAD ignition system. It consists of the Pad-Box and the ground station which are connected via radio link. With the elaborated implemented safety system, it allows us to ignite the rocket safely from a distance over a few kilometers.

Another achievement is the evolved and improved SRAD flightcomputer. With a few very important peripherals like the recovery pressure sensors or the instrumented solid booster and sensor fusion from the flightcomputer data, we collect more and higher quality data than before. This is also crucial for further development.

This year's SRAD single-grain finocyl solid booster is a completely new design for more reliability and safety, and has an improved burn rate. Also, the manufacturing process was evolved to be less complex and therefore having a consistently better fuel grain quality.

In conclusion, both from a technical and organizational standpoint, the AVES II project has definitely been demanding but also rewarding at the same time already now before the launch. In comparison to last year's AVES project, the fact, that we had more than double the project time definitely helped to spend more time on the design process but more importantly on testing. Some challenges we have faced include long waiting times due to chip shortages and material delivery bottlenecks. A goal for this project was to have a test flight to the full 3 km apogee before the EuRoC in October. However, bureaucracies of any kind impeed undertakings such as the planned flight test. Finding potential launch sites as well as an insurance to legally conduct a rocket launch almost seems to be impossible. Nevertheless, we are continuing our efforts to arrange this flight before the EuRoC in October 2022. Even if we cannot launch before October, we hope that we will be able to launch AVES II and future rockets in Austria at some point.

Appendices

A. Acronyms

ABS Acrylnitril-Butadien-Styrol

ADC Analog-to-Digital Converter

AIR-S airbrake section

AoA Angle of attack

APRS Automatic Packet Reporting System

ARM Advanced RISC Machines

ASTG Aerospace Team Graz

AVI Avionics

AVI-S avionics section

AW Aluminium Wrought

brcc burn-rate-coefficient coefficient

BTN Button

CAD Computer Aided Design

CAS Control Actuator Systems

CCC Cropped Combustion Chamber

CeFRP ceramic-fibre-reinforced-polymer

CFD Computational Fluid Dynamics

CFRP carbon-fibre-reinforced-polymer

CoG Centre of Gravity

CONOPS Mission Concept of Operations

COTS Commercial Off The Shelf

EMI Electro-Magnetic-Interference

EN European Norm

ESA Space Solutions Austria European Space Agency Space Solutions Austria

EuRoC European Rocketry Challenge

FEA Finite Element Analysis

FPM Fluorinated Rubber

FSK Frequency-Shift Keying

GFRP glass-fibre-reinforced-polymer

GNSS Global Navigation Satellite System

IC Integrated Circuit

IFT Institute of manufacturing engineering

IGN Ignition

IIM Institute of Innovation and Industrial Management

IMU Inertial Measurement Unit

KNO_3 Potassium Nitrate

KEY Keyswitch

LiPo Lithium-Polymer

LIT Light lit

LoRa Long Range

Max Q Maximum Dynamic Pressure

MCU Micro Controller Unit

MoI Moment of inertia

µCT Micro Computed Tomography

NC Nitrocellulose

NC-CT nose cone coupling tube

NC-S nosecone section

PA 12 Polyamid 12 / Nylon 12

PBO Poly(p-phenylen-2,6-benzobisoxazol, trade name Zylon ©)

PC Polycarbonate

PCB Printed Circuit Board

PI Proportional Integral

PRO-S booster section

PSU Power Supply Unit

PTFE Polytetrafluoroethylene

PU Polyurethane

RC Rocket Candy

REC-S recovery section

RF Radio Frequency

RTOS Real Time Operating System

SD Secure Digital

SDR Software Defined Radio

SLS Sodium Laureth Sulfate

SPI Serial Peripheral Interface

SRAD Student Researched And Developed

SRS - TD Solid Rocket Simulation - Time Driven

SWR Standing Wave Ratio

SW Switch

TC tailcone

TEL Telemetry

TUG University of Technology Graz

UART Universal Asynchronous Receiver Transmitter

VSWR Voltage Standing Wave Ratio